THE JOURNAL OF BIOLOGICAL CHEMISTRY VOL. 289, NO. 4, pp. 2261–2276, January 24, 2014

Collapsin Response Mediator Protein 5 (CRMP5) Induces Mitophagy, Thereby Regulating Mitochondrion Numbers in Dendrites

Received for publication, June 4, 2013, and in revised form, December 6, 2013 Published, JBC Papers in Press, December 9, 2013, DOI 10.1074/jbc.M113.490862

Sébastien Brot[‡§¶], Carole Auger[‡§¶], Rabia Bentata[‡§¶], Véronique Rogemond[‖], Stéphane Ménigoz[‡§¶], Naura Chounlamountri[‡§¶], Agnès Girard-Egrot**, Jérôme Honnorat[‡§¶‖], and Mahnaz Moradi-Améli[‡§¶1]**

*From [‡]INSERM, UMR-S1028, [§]CNRS, UMR5292, and [¶]University Lyon 1, University Lyon, Lyon Neuroscience Research Center, Rue Guillaume Paradin, Lyon Cedex 08, F-69372 France, [‖]Hospices Civils de Lyon, Neuro-oncologie, Bron F-69677, France, and **Institut de Chimie et Biochimie Moléculaires et Supramoléculaires, CNRS UMR 5246 ICBMS, University Lyon 1, Villeurbanne Cedex, F-69622 France*

Background: Collapsin response mediator protein 5 (CRMP5) influences neuronal differentiation and dendrite outgrowth during brain development.
Results: CRMP5 is partially located in mitochondrial membranes, inducing mitophagy and reducing mitochondrial content of developing dendrites.
Conclusion: Control of mitochondrion numbers by CRMP5 inhibits dendrite growth when the axon is growing.
Significance: Learning how dendrite growth is regulated by CRMP5 is important for understanding the establishment of neuronal polarization.

Degradation of damaged mitochondria by mitophagy is an essential process to ensure cell homeostasis. Because neurons, which have a high energy demand, are particularly dependent on the mitochondrial dynamics, mitophagy represents a key mechanism to ensure correct neuronal function. Collapsin response mediator proteins 5 (CRMP5) belongs to a family of cytosolic proteins involved in axon guidance and neurite outgrowth signaling during neural development. CRMP5, which is highly expressed during brain development, plays an important role in the regulation of neuronal polarity by inhibiting dendrite outgrowth at early developmental stages. Here, we demonstrated that CRMP5 was present *in vivo* in brain mitochondria and is targeted to the inner mitochondrial membrane. The mitochondrial localization of CRMP5 induced mitophagy. CRMP5 overexpression triggered a drastic change in mitochondrial morphology, increased the number of lysosomes and double membrane vesicles termed autophagosomes, and enhanced the occurrence of microtubule-associated protein 1 light chain 3 (LC3) at the mitochondrial level. Moreover, the lipidated form of LC3, LC3-II, which triggers autophagy by insertion into autophagosomes, enhanced mitophagy initiation. Lysosomal marker translocates at the mitochondrial level, suggesting autophagosome-lysosome fusion, and induced the reduction of mitochondrial content via lysosomal degradation. We show that during early developmental stages the strong expression of endogenous CRMP5, which inhibits dendrite growth, correlated with a decrease of mitochondrial content. In contrast, the knockdown or a decrease of CRMP5 expression at later stages enhanced mitochondrion numbers in cultured neurons, suggesting that CRMP5 modulated these numbers. Our study elucidates a novel regulatory mechanism that utilizes CRMP5-induced mitophagy to orchestrate proper dendrite outgrowth and neuronal function.

Mitophagy is a regulated catabolic mechanism whereby cells degrade their damaged mitochondria via autophagy (1–3). This process seems to be the primary mechanism to ensure mitochondrial quality control that protects cells from damaged mitochondria and from the release of potentially proapoptotic molecules (4–6). However, mitophagy is also an actor in the removal of undamaged mitochondria during developmental stages to regulate the changes in steady-state mitochondrial number (6). The process of autophagic degradation is initiated by the sequestration of cytosolic components, such as mitochondria, into double membrane vesicles termed autophagosomes. Many autophagy-related genes (*Atg*),[2] identified in yeast, are thought to play similar roles in mammalian cells. Among them, *Atg12* and *Atg8* (LC3 counterparts in mammals) are crucial for autophagy (7). As for Atg8, the conversion of cytosolic LC3-I to phosphatidylethanolamine-conjugated LC3-II in mammalian cells contributes to the formation of autophagosomes and the activation of autophagy (7, 8). Autophagosomes in turn fuse with endosomes and/or lysosomes to form autolysosomes for the hydrolytic degradation of

[1] To whom correspondence should be addressed: Lyon Neuroscience Research Center, Université Lyon 1, Faculté de Médecine Lyon-Est, Rue Guillaume Paradin, 69372 Lyon Cedex 08, France. Tel.: 33-478-771058; Fax: 33-478-778616; E-mail: mahnaz.ameli-moradi@univ-lyon1.fr.

[2] The abbreviations used are: Atg, autophagy-related gene; CRMP5, collapsin response mediator protein 5; DMPC, 1,2-dimyristoyl-*sn*-glycero-3-phosphocholine; DRP-1, dynamin-related protein-1; LAMP-2, lysosome-associated membrane protein-2; LC3, microtubule-associated protein 1 light chain 3; $\Delta\Psi_m$, mitochondrial membrane potential; PINK1, PTEN (*phosphatase and tensin homolog*)-induced putative kinase 1; MAP2, microtubule-associated protein 2; COX IV, cytochrome *c* oxidase subunit IV; DMPE, 1,2-dimyristoyl-*sn*-glycero-3-ethanolamine; π_i, initial surface pressure; $\Delta\pi$, surface pressure increase; mN, millinewton(s); DIV, day(s) of *in vitro* culture; MT, MitoTracker CMXRos; SC, control RNA; siCRMP5, CRMP5 siRNA; E18, embryonic day 18; P8, postnatal day 8; a.u., arbitrary units.

sequestered material (7). Resulting macromolecules are then transported back into the cytosol for reuse. Whether the autophagic pathway exerts anti- or prodeath roles in neurons under pathological conditions remains unclear (9). Nevertheless, it is increasingly accepted that correct neuronal function is dependent on the trafficking and dynamics of mitochondria, and disruptions in mitochondrial function lead to various neurodegenerative disorders (10, 11), such as Parkinson disease (2). Studies on the molecular mechanisms underlying mitophagy have led to the identification of new proteins involved in mitochondrial dynamics. Dynamin-related protein-1 (DRP-1) promotes mitochondrial fission upon recruitment to the outer mitochondrial membrane (12). The protein Parkin, which is commonly mutated in Parkinson disease, translocates to mitochondria after dissipation of the mitochondrial membrane potential ($\Delta\Psi_m$) and ensures the removal of damaged mitochondria via mitophagy (2, 13, 14). Other proteins interacting with or functioning in the same pathway as Parkin, such as the PTEN-induced putative kinase 1 (PINK1) and Nix (15, 16), have been identified.

Collapsin response mediator proteins (CRMPs) are a family of five cytosolic proteins (CRMP1–5) that are highly expressed in the developing brain (17, 18). CRMPs act as signaling molecules involved in the regulation of microtubule polymerization, actin bundling, and endocytosis, leading to neuronal differentiation. CRMP2 was originally identified as the intracellular mediator of Semaphorin 3A signaling that induces growth cone collapse (19). It is now accepted that CRMP2, the best studied member of the CRMP family, is involved in different functions, such as the regulation of neuronal polarity, axon elongation, vesicle trafficking, and synaptic physiology (20–22). Fewer studies relate to CRMP5, which is highly expressed in developing brain but decreases in adult brain because at postnatal stages its expression is restrained to the brain areas that retain neurogenesis (23). CRMP5 exhibits spatiotemporal expression in the cortex, hippocampus, and cerebellum and in the postmitotic neuronal precursors, suggesting that it plays a role in process extension (24). Another study has reported that it exerts a role in the regulation of filopodial dynamics and growth cone development (25). The results obtained recently with CRMP5-deficient mice stress the role of CRMP5 in the development and synaptic plasticity of cerebellar Purkinje cells (26). We reported CRMP5 inhibition of neurite outgrowth, especially at the dendritic level, by forming a complex with tubulin and microtubule-associated protein 2 (MAP2). Interestingly, the neurite outgrowth-promoting function of CRMP2 is totally abrogated by CRMP5, which acts as the dominant signal (27). Very recently, the crystal structure of CRMP5 was elucidated, pointing out the homotetramerization of the protein but also that it can compete and interact essentially with CRMP2 (28). On the other hand, anti-CRMP5 antibody has been recognized as one of the main antibodies associated with paraneoplastic neurological syndromes as a result of a cancer-induced autoimmune process (29). In this study, we identified a new function for CRMP5 as an actor in the mitophagic pathway. We demonstrate for the first time that CRMP5 was present *in vivo* in brain mitochondria and that its overexpression triggered a drastic change in mitochondrial morphology and an increase in LC3-II expression, suggesting the initiation of autophagic processes. Besides, CRMP5 overexpression caused an increase of lysosomal markers recruited at the mitochondrial level, leading to a decrease of mitochondrion numbers. In hippocampal neurons, the endogenous high CRMP5 expression correlated with a decrease of mitochondrial number, regulating the metabolic demand and ensuring proper neuronal function during developmental stages.

EXPERIMENTAL PROCEDURES

Subcellular Fractionation from Mouse Brain—Cortex, cerebellum, and brain stem of postnatal mouse (P8) were explanted, cleaned free of meninges, and subjected to subcellular fractionation using the ProteoExtract subcellular proteome extraction kit (Calbiochem) as described previously (30).

Antibodies Used and Western Blot Analysis—The site-specific antibody to CRMP5 (anti-CRMP5 antibody) was produced in rabbits, and the specificity of the purified antibody toward CRMP5 was checked as described previously (24). Other antibodies used were anti-COX IV (ab16056, Abcam), anti-calpain (H-65, Santa Cruz Biotechnology), anti-Tim23 (611223, BD Biosciences), anti-Tom20 (Santa Cruz Biotechnology), anti-HA (clone HA-7, Sigma-Aldrich), anti-neurofilament (AHP245, Serotec), anti-FLAG (clone M2, Sigma-Aldrich), anti-LC3 (2775, Cell Signaling Technology), anti-DRP-1 (611738, BD Biosciences), anti-Parkin (clone PRK8, Sigma-Aldrich), anti-lysosome-associated membrane protein-2 (LAMP-2) (GL2A7, Abcam), anti-cytochrome *c* (H-104, Santa Cruz Biotechnology), anti-GAPDH (MAB374, Millipore), anti-MAP2 (Sigma-Aldrich), and anti-tau-1 (H-150, Santa Cruz Biotechnology) antibodies. Subcellular fractions from mouse brain or cell lysate were resolved by SDS-PAGE, transferred to a nitrocellulose membrane, and incubated with different antibodies as described (30). An equal amount of protein (76 μg) was loaded for mitochondrial and cytosolic fractions, which represented 20 and 2.5% of total mitochondrial and cytosolic preparations, respectively.

Recombinant Protein Production and Lipid Insertion Measurement—The cDNA encoding full-length human CRMP5 (residues 1–564) or a truncated form of the protein (residues 1–520) was inserted into the pT7-7 expression vector, which generated a protein with six His residues at its C terminus. The recombinant proteins were produced and purified as described previously (27). The Wilhelmy balance method was used to measure protein-induced changes in the surface pressure of a monomolecular film of phospholipids at constant surface area. A monomolecular film was performed by spreading the phospholipid 1,2-dimyristoyl-*sn*-glycero-3-phosphocholine (DMPC) or 1,2-dimyristoyl-*sn*-glycero-3-ethanolamine (DMPE) dissolved in chloroform/methanol (9:1, v/v) on the buffer subphase (20 mM Tris-HCl, pH7.5, 0.15 M NaCl, 1 mM dithiothreitol (DTT)). After complete solvent evaporation, the monolayer was slowly compressed up to a defined lateral pressure (initial surface pressure (π_i)). A 10-min lag time was necessary for the monolayer relaxation and for checking the monolayer stability. CRMP5 protein was then injected into the buffer subphase gently stirred with a magnetic bar between fixed barriers (imposing a constant area), in a controlled atmosphere, and at constant temperature (22 °C). The surface pressure increase

produced by protein insertion in the monolayer was recorded using a Wilhelmy balance with an accuracy of ± 0.05 mN/m as described (31).

Isolation of Mitochondria and Various Treatments—Mitochondria and cytosol were isolated from postnatal mouse cortex (P8) or from COS-7 cells using the mitochondria isolation kit for tissue or cultured cells, respectively, as indicated by the manufacturer (Pierce). The mitochondria were treated with trypsin or trypsin and digitonin as follows. Isolated mitochondria were suspended in buffer A (70 mM sucrose, 220 mM D-mannitol, 2.5 mM Hepes, pH 7.4) to achieve a final concentration of about 350 μg/ml. Trypsin was added to the mitochondrial fraction at the indicated concentrations and incubated at room temperature for varying amounts of time. The reaction was stopped by the addition of Laemmli buffer and heating for 5 min at 90 °C. For trypsin plus digitonin digestion, the non-ionic detergent was added to the mitochondrial fraction at a final concentration of 1 or 5 mg/ml for 10 min at 4 °C. Four volumes of buffer A were then added to the sample followed by centrifugation at 13,000 × *g* at 4 °C for 10 min. The pellets containing the mitoplasts were incubated with trypsin as described above and resuspended in Laemmli buffer before electrophoresis and Western blotting. For carbonate extraction, mitochondria were first treated with digitonin at 5 mg/ml for 10 min. After centrifugation, the pellet was incubated for 20 min in 0.1 M Na_2CO_3 at 4 °C, and then the sample was centrifuged at 13,000 × *g* at 4 °C for 10 min. The supernatant was neutralized with 25% HCl, and the pellet was rinsed once with 20 mM Tris-HCl, pH 7.5, 1 mM EDTA; 1 mM EGTA, 1 mM DTT before Western blot analysis.

For combined trypsin digestion with Triton X-100, Triton (0.3%) was added and incubated for 5 min with the mitochondrial preparation prior to incubation with increasing concentrations of trypsin for 5 min at 30 °C and Western blotting. In some experiments, the mitochondrial pellet was resuspended in hypotonic buffer containing 20 mM Hepes, pH 7.4 to obtain swelled mitochondria following incubation with 5 μg/ml trypsin at 30 °C for varying amounts of time. After centrifugation at 13,000 × *g* at 4 °C for 10 min, the pellet containing mitoplasts was analyzed by Western blotting.

Expression Constructs and Transfection—N-terminally FLAG-tagged full-length CRMP5 was obtained as described previously (27). cDNA fragments encoding full-length human CRMP5 or different truncated mutants (CRMP5 ΔN104, CRMP5 ΔN285, CRMP5 ΔN300, and CRMP5 ΔC508) were sequentially ligated into pCEFL-tagged HA vectors within EcoRI and NotI restriction sites, generating a protein with an HA tag at its N terminus. All fragments were confirmed by DNA sequencing. Cells were transfected using Lipofectamine LTX (Invitrogen) and fixed for immunostaining or disrupted in lysis buffer at 48 h post-transfection as described (27). In some experiments, at 46 h post-transfection, COS-7 cells were incubated with bafilomycin A1 (Sigma-Aldrich) at a final concentration of 10 nM for 2 h before disruption in lysis buffer for Western blotting. PC12 cells were stimulated by 100 ng/ml NGF 8 h after transfection.

Primary Culture of Hippocampal Neurons—Hippocampal neurons from embryonic day 18 (E18) mouse embryos were prepared and plated at a density of 5 × 10^4 cells/well as described (27) and fixed after MitoTracker staining (see below) on days 2–5 of *in vitro* culture (DIV 2–5).

Immunocytochemistry, Microscopy Observation, and Morphology Assay—For mitochondrial staining, the cells were incubated with 200 nM MitoTracker CMXRos (MT; Invitrogen) for 25 min before fixation. PC12 cells were incubated with anti-CRMP5 followed by anti-rabbit Alexa Fluor 488 (Invitrogen) antibodies for endogenous CRMP5 staining. PC12 cells were observed using a laser-scanning confocal system (Leica TCF SP2 imaging platform). SH-SY5Y cells were immunostained with anti-FLAG followed by anti-mouse Alexa Fluor 488 antibodies added after MT staining. COS-7 cells were immunostained with anti-HA and anti-mouse Alexa Fluor 488 (Invitrogen) antibodies or anti-FLAG followed by either anti-mouse or anti-rabbit Alexa Fluor 488 antibodies. For double staining, in addition to anti-FLAG labeling, the cells were stained with anti-Parkin, anti-DRP-1, or anti-LC3 followed by anti-mouse or anti-rabbit Alexa Fluor 555 (Invitrogen) antibodies. In some experiments, COS-7 cells were double stained with anti-LAMP-2 and anti-cytochrome *c* followed by anti-rat Alexa Fluor 488 and anti-rabbit Alexa Fluor 555 antibodies, respectively. COS-7 cells were observed using an Axioplan II fluorescence microscope with an apotome (Carl Zeiss). For LC3 fluorescence quantification, the green fluorescence intensity of an individual cell was obtained using AxioVision Rel.4.8 software, and the mean fluorescence values of LC3-positive cells (CRMP5-transfected cells) were expressed compared with the control cells.

Hippocampal neurons were stained with MT, then fixed, and stained with anti-CRMP5 followed by anti-rabbit Alexa Fluor 488 antibodies at DIV 2–5. Images of fluorescent neurons were captured with a fluorescence microscope. The longest neurite was considered as axon, and the remaining shorter neurites of an individual neuron were considered as dendrites. To determine the fluorescence intensity, all fluorescent images were digitally converted into a grayscale image before analysis. Quantitative measurements of fluorescence intensities were done by averaging the intensity within a square box of 40 × 40 pixels in size obtained from a defined area across axon and dendrites, but not cell bodies, using image processing ImageJ 1.42q software as described (27). The grayscale intensity was corrected against the intensity point of the background. Numerical fluorescence values were graphed as fluorescence intensity for CRMP5 or mitochondria at DIV 2–5.

Knockdown of Gene Expression by Small Interfering RNA in Culture of Hippocampal Neurons—Validated siRNA against CRMP5 sequence (25) and control RNA (SC; scrambled sequence with the same percentage of CG without sequence homology) were purchased from Invitrogen. Cultured hippocampal neurons were transfected 24 h after plating with 100 nM CRMP5 siRNA (siCRMP5) or SC using a Ribojuice kit according to the manufacturer's instructions (Novagen). At 48 h post-transfection, corresponding to DIV3, neurons were first labeled with 200 nM MT, then fixed, stained with anti-CRMP5 antibody, and observed with an Axioplan II fluorescence microscope with apotome (Carl Zeiss). To ensure correct comparison of the labeling between different transfections, the acquisition of each picture was realized with the same exposure

time (300 ms for CRMP5 green labeling and 350 ms for MT). The number of mitochondria in axon and dendrites of each neuron was individually counted using AxioVision Rel.4.8 software.

Electron Microscopy—COS-7 cells transfected with FLAG or FLAG-CRMP5 vectors were fixed with 2.5% glutaraldehyde, 0.1 M sodium cacodylate, pH 7.3 for 45 min. They were postfixed with 1% OsO_4 in 0.15 M sodium cacodylate, pH 7.3. After dehydrating with a graded ethanol series, they were embedded in Epon resin. Cell sections were collected on nickel grids. Grids were incubated with anti-FLAG followed by 18-nm gold-IgG anti-mouse (Jackson ImmunoResearch Laboratories) antibodies. Contrast was obtained by uranyl acetate incubation. Cells were examined with a transmission electron microscope (JEOL JEM 1400, Cecil, Lyon, France) and photographed at various magnifications.

Statistical Analysis—Differences between means were compared using unpaired two-tailed Student's *t* test. Data were reported as mean ± S.E. with $p < 0.01$ considered as the level of significance. Data are the mean values of at least three individual experiments.

RESULTS

Subcellular Localization of CRMP5 in Mitochondria—To understand CRMP5 function during brain development, we studied its subcellular localization. Subcellular fractionations from the cortex, cerebellum, and brain stem of developing mouse brain (P8) were subjected to Western blot analysis. Besides its cytosolic distribution, CRMP5 was clearly present in the membrane fraction (Fig. 1*A*). Antibodies specific to each fraction were used to check the purity of the fractionations. The membrane insertion property of the CRMP5 was stressed by studying the interaction of purified recombinant protein with a lipid monolayer of DMPC or DMPE. The interaction was analyzed using Langmuir film balance technology based on the phospholipid displacement in monolayers. In these experiments, full-length or truncated (ΔC520) recombinant CRMP5 was injected, using a constant area setup, into the aqueous sub-

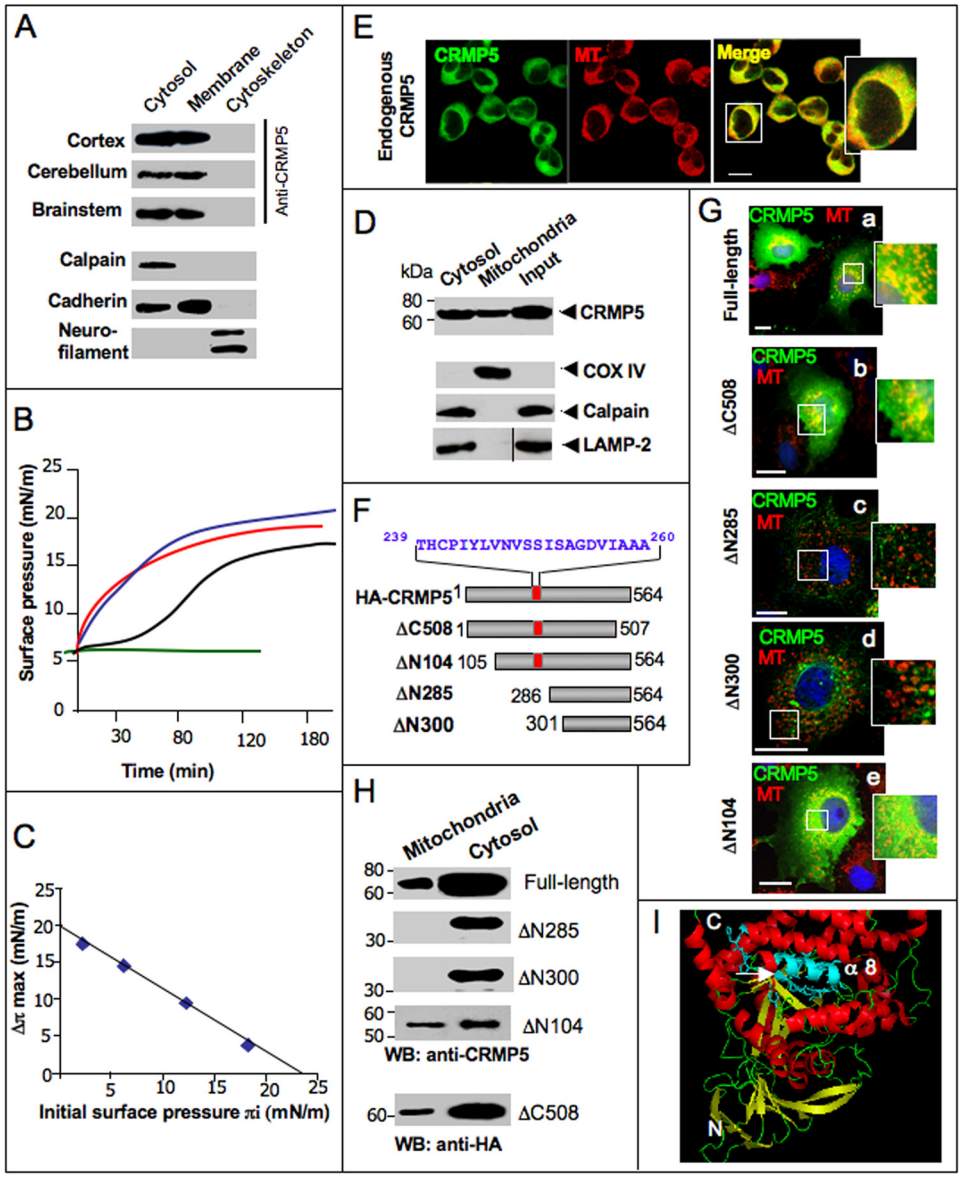

phase underneath the phospholipid monolayer. The resulting interaction was measured as the surface pressure increase ($\Delta\pi$) of the film, reflecting the insertion of proteins between phospholipid molecules. CRMP5 insertion into DMPC monolayer gave rise to an immediate surface pressure increase (Fig. 1*B*, *blue line*), whereas no surface pressure change was observed upon injection of the buffer in which CRMP5 was stored (Fig. 1*B*, *green line*). The increase in surface pressure was identical for the full-length and C-terminally truncated ΔC520 CRMP5 proteins (Fig. 1*B*, *red line*), indicating that the C-terminal part of the protein was not involved in its membrane insertion. The insertion of full-length CRMP5 resulted in a slightly higher surface pressure change in DMPC than in DMPE monolayer (Fig. 1*B*, *black line*), indicating the specificity of the interaction with mitochondrial membrane, which contains mostly zwitterionic phospholipids (phosphatidylcholine headgroup) and a small percentage of negatively charged lipids (32). Also, it is worthwhile noting that CRMP5 insertion into DMPE is clearly slower than in DMPC monolayer. Besides, DMPC monolayers were prepared at various π_i values, and $\Delta\pi$ induced by phosphatidylcholine insertion of CRMP5 was measured to determine the penetrative power of the protein. Fig. 1*C* shows that $\Delta\pi$ gradually decreased as π_i increased. The maximal pressure insertion (*i.e.* the theoretical value of π_i extrapolated for $\Delta\pi = 0$ mN/m) was 23 mN/m. This influence of the initial packing density of the monolayer on CRMP5 penetration demonstrates a direct CRMP5/lipid interaction as evidenced for other lipids and ligands (31, 33).

The presence of CRMP5 in mitochondria was further confirmed after purification of mitochondria isolated from the cortex of P8 mouse brain. Postnatal mouse brains were used in this study because CRMP5, which is involved in developmental processes, is slightly expressed in adult brain. Western blot analysis using anti-CRMP5 antibody showed that CRMP5 was clearly detected not only in the cytosolic fraction but also in the mitochondrial fraction (Fig. 1*D*, *upper panel*). The anti-COX IV antibody, which labels the mitochondrial cytochrome *c* oxidase, and anti-calpain antibody, which labels the cytosol, confirmed the purity of the mitochondrial and cytosolic fractions, respectively. In addition, the absence of staining of the mitochondrial fraction with lysosomal marker LAMP-2 ascertained that mitochondria were not contaminated with lysosomal fraction (Fig. 1*D*, *lower panels*). When, instead of an equivalent amount of protein as above, an identical proportion (equal volume) of the mitochondrial and cytosolic fractions from the cortex of P8 mouse brain was used in Western blot analysis, the proportion of CRMP5 in brain cortex that lodged in the mitochondrial fraction and cytosol was 15 and 85%, respectively, of the total protein (data not shown). To further confirm the localization of CRMP5 in mitochondria, the endogenous CRMP5 distribution was examined using CRMP5 antibody in NGF-stimulated PC12 cells, which present a neuronal phenotype. We found punctate labeling (stained *green*) reminiscent of mitochondrial staining overlapping with the *red* MT labeling (Fig. 1*E*). It should be noted that non-overlapped *green* and *red* staining could also be distinguished. The CRMP5 mitochondrial localization was also observed in HA-tagged CRMP5 overexpressed in COS-7 cells stained with MT (*red*) and anti-HA antibody (*green*) as shown by the *yellow* staining in the merged image (Fig. 1*G*, *panel a*). Similar results were obtained with other cell lines (data not shown), indicating mitochondrial localization for CRMP5. All together, those experiments indicate that CRMP5 is located in brain mitochondria although in a low proportion in P8 mouse cortex. This is the first report on the mitochondrial localization of CRMP5 *in vivo*.

The N-terminal CRMP5 Domain Controls Mitochondrial Targeting—To determine the CRMP5 domain responsible for its mitochondrial localization, we designed several dele-

FIGURE 1. **CRMP5 presents membrane insertion capacity and mitochondrial localization.** *A*, Western blot analysis of different subcellular fractions from the cortex, cerebellum, and brain stem of P8 mouse brain. Aliquots were separated by SDS-PAGE, and CRMP5 expression was probed by anti-CRMP5 antibody. The representative image (from three different experiments) shows the presence of CRMP5 in the cytosolic fraction but also in the membrane fraction of the three tissues. CRMP5 is absent from the cytoskeletal fraction. The *bottom panels* show the identification of each subcellular fraction using anti-calpain for cytosol staining, anti-cadherin for membrane labeling, and anti-neurofilament for intermediate filament staining. Note that anti-cadherin also detects the cytosolic fraction. *B*, time course of the monolayer insertion of CRMP5. Full-length CRMP5 was injected underneath the monolayer of either DMPC (17 nmol; *blue*) or DMPE (22 nmol; *black*) at a π_i of 6 mN/m. ΔC520 recombinant CRMP5 (*red*) was injected underneath DMPC monolayer under identical conditions. The final concentration of each protein was 4.5 nM. Changes in surface pressure were recorded at constant area and temperature 22 °C. Upon injection of the buffer in which CRMP5 was stored, no change in surface pressure is observed (*green*). An immediate increase of surface pressure was recorded with $\Delta\pi_{max}$ of ≈20 mN/m for full-length and ΔC520 CRMP5, indicating rapid DMPC monolayer insertion of the proteins. The kinetics of CRMP5 insertion into DMPE monolayer was rather sigmoid with an inflection point around 10 mN/m, and the $\Delta\pi_{max}$ reached 17 mN/m, indicating a lower insertion capacity of CRMP5. *C*, different monolayers of DMPC were prepared at various π_i values, and then the $\Delta\pi$ induced by CRMP5 (5.3 nM) was determined following attainment of equilibrium. Higher initial monolayer surface pressure correlates with higher lipid packing densities and reduces the penetrative power of the protein. Each point is an independent measurement with a new lipid monolayer. Representative data from two independent experiences are shown. *D*, Western blot analysis shows the presence of CRMP5 protein in the cytosolic fraction as well as in mitochondria isolated from P8 mouse cortex. The *bottom panels* show the Western blot of each fraction probed with anti-COX IV and anti-calpain antibodies to identify the mitochondrial and cytosolic fractions, respectively. The absence of COX IV staining in the cytosol could be explained by its low amount in the whole lysate compared with isolated mitochondria. Note the absence of the lysosomal marker LAMP-2 in the purified mitochondrial fraction. *E*, NGF-stimulated PC12 cells, presenting a neuronal phenotype, were stained with MT to label coupled mitochondria. The cells were then fixed before immunostaining with anti-CRMP5 antibody. The *yellow* color in the merge image indicates the co-localization of CRMP5 and MT. The *right panel* shows high magnification of the *boxed areas*. Cells were observed by confocal microscopy. *Scale bars*, 10 μm. *F*, diagram depicting CRMP5 truncation mutants with the putative hydrophobic domain (residues 239–260) shown by a *red box*. *G*, *panels a–e*, immunofluorescence of COS-7 cells transfected with the different HA-tagged CRMP5 constructs shown in *F*. At 48 h post-transfection, the cells were incubated with MT, then fixed, and immunostained with anti-HA antibody. The nucleus is stained *blue* with DAPI. *Insets* represent high magnification of the mitochondria. *Yellow* spots in the representative fluorescence microscopy image indicate the co-localization of CRMP5 (*green*) and mitochondria (*red*). The images are representative of three separate experiments with similar results. *Scale bars*, 20 μm. *H*, mitochondria were isolated from COS-7 cells transfected with mutated HA-CRMP5 constructs. Mitochondrial and cytosolic fractions were subjected to SDS-PAGE and Western blotting (*WB*). The Western blots in the *three upper panels* were probed with anti-CRMP5 antibody. Due to the absence of the antigenic site recognized by the anti-CRMP5 antibody on the ΔC508 mutant, in the *lower panel*, the blot was probed by anti-HA antibody. The *bars* to the *left* of the panels show the molecular marker masses in kDa. *I*, a ribbon diagram showing one monomer within the dimer structure of CRMP5 according to coordinates available for CRMP5 (Protein Data Bank code 4B90). Residues 239–260 located on β-strand 15 (*white arrow*) and α-helix 8 are colored *blue*. Both structures, especially β-strand 15, seem to be buried in the interior of the molecule.

tion constructs of CRMP5 (Fig. 1*F*). Because the C-terminal part of CRMP5 was reported to bind tubulin (27), to avoid any disturbance in its tubulin-binding capacity, the N-terminally HA-tagged CRMP5 was used. We performed a series of transfections in COS-7 cells with either full-length or mutated CRMP5 truncated at its N-terminal (CRMP5 ΔN104, ΔN285, and ΔN300) or C-terminal parts (CRMP5 ΔC508). In accordance with the above mentioned lipid insertion property of CRMP5, the full-length and the C-terminally deleted mutant CRMP5 ΔC508 presented both mitochondrial and cytosolic distributions (Fig. 1*G*, *panels a* and *b*). On the contrary, both N-terminally deleted mutants (CRMP5 ΔN285 and CRMP5 ΔN300) did not exhibit any mitochondrial localization because distinct *red* (MT) and *green* (CRMP5) staining was observed (Fig. 1*G*, *panels c* and *d*). However, the most N-terminally deleted mutant, ΔN104, exhibited a clear mitochondrial distribution (Fig. 1*G*, *panel e*). To strengthen these results, mitochondria were isolated from cells transfected with different constructs and subjected to Western blot analysis (Fig. 1*H*). Although both CRMP5 ΔN285 and ΔN300 were totally absent in the mitochondrial fraction, the presence of full-length and mutant CRMP5 ΔC508 and ΔN104 was clearly observed in the isolated mitochondria. Note the presence of all constructs in the cytosolic fraction. These data unambiguously show that an internal fragment within the N-terminal part of the CRMP5 protein (residues 105–285) is essential for its targeting to mitochondria. Within this fragment, a potential hydrophobic domain within residues 239–260 located on β-strand 15 and α-helix 8 of the CRMP5 structure can be distinguished (28). As for all hydrophobic domains, both structures seemed to be buried in the interior of the molecule, in particular β-strand 15 (Fig. 1*I*, *white arrow*), suggesting that CRMP5 might undergo a conformational change, exposing this fragment for membrane insertion.

Submitochondrial Location of CRMP5—To acquire more insight on the localization of CRMP5 within mitochondria, we examined its submitochondrial localization in isolated mitochondria from brain. We assessed the accessibility of the protein to trypsin digestion under various conditions. Treating isolated mitochondria with a high trypsin concentration such as 400 μg/ml for 40 min at room temperature did not affect the presence of CRMP5 in mitochondria (Fig. 2*A*), suggesting that CRMP5 was not accessible to trypsin and consequently not oriented to the outside, *i.e.* cytosolic side, of the outer mitochondrial membrane. However, when mitochondrial fractions were first incubated with digitonin for 10 min to destabilize the outer membrane, CRMP5 protein began to be degraded by tryptic digestion, showing lower molecular mass after 10 min of treatment and almost disappearing after 20 min of incubation, indicating that this treatment enhanced the accessibility of CRMP5 protein to tryptic digestion (Fig. 2*A*). It should be noted that CRMP5 was resistant to digitonin treatment alone (data not shown). These data suggested that CRMP5 might be oriented toward the intermembrane space. CRMP5 was easily digested by trypsin at concentrations as low as 2 μg/ml when solubilized by Triton X-100, indicating that it interacted with the mitochondrial membrane (Fig. 2*B*). Incubation of isolated mitochondria in hypotonic swelling conditions removed the outer

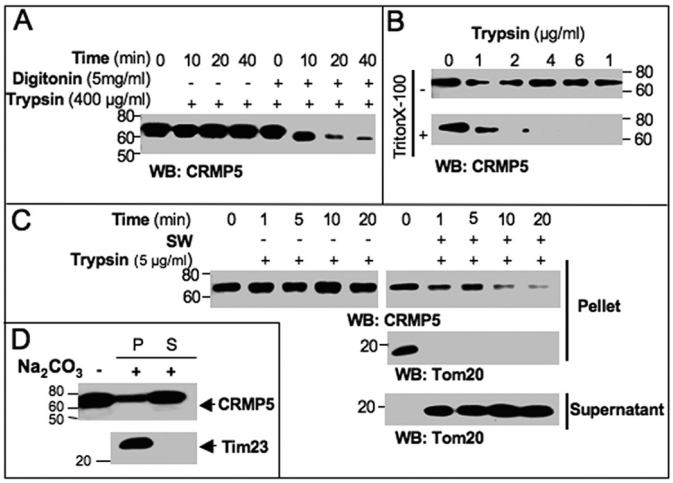

FIGURE 2. **Characterization of mitochondrial CRMP5 topology.** *A–C*, trypsin sensitivity of mitochondrial CRMP5. *A*, time course proteolysis of mitochondria in the presence or absence of 5 mg of digitonin/ml. After 10 min of digitonin treatment following 10 min of centrifugation at 13,000 × *g*, trypsin was added to the pellet at a concentration of 400 μg/ml. CRMP5 became sensitive to trypsin attack after digitonin treatment. *B*, proteolysis of isolated mitochondria treated or not with 0.3% Triton X-100. After 5 min, increasing concentrations of trypsin were added, and the mitochondria were incubated at 30 °C for an additional 5 min. Western blot (*WB*) analysis shows that after membrane solubilization by Triton X-100 CRMP5 becomes sensitive to proteolytic attack even at a very low concentration (2 μg trypsin/ml). *C*, time course proteolysis of mitochondria in isotonic (*SW* −) or hypotonic (*SW* +) buffer. *SW*, swell mitochondria. Trypsin was added at a concentration of 5 μg/ml. The removal of the outer mitochondrial membrane under hypotonic conditions was shown by the absence of Tom20 immunostaining in the pellet. CRMP5 remains in the pellet and is resistant to trypsin proteolysis for the first 5 min, but it shows sensitivity to proteolysis after 10 min of treatment. In *A–C*, immunoblots were probed with antibodies as indicated at the *bottom* of each panel. The *bars* at the *left* or *right* of each panel show the mass of the molecular markers in kDa. *D*, carbonate extraction assay. Mitochondria were incubated for 10 min in the presence of 5 mg digitonin/ml. After centrifugation, carbonate extraction was carried out on the pellet for 20 min in 0.1 M Na_2CO_3. Another centrifugation at 13,000 × *g* for 10 min allowed the separation of the pellet (*P*; integral protein) and supernatant (*S*; peripheral protein) fractions. The presence of Tim23 in the pellet, but not in the supernatant, confirmed the identity of the fraction as integral inner mitochondrial membrane proteins.

mitochondrial membrane as evidenced by the absence of a marker of the mitochondrial outer membrane, Tom20, in the pellet and its presence in the supernatant (Fig. 2*C*, *right panels*). In such swelling conditions, CRMP5 remained in the pellet in the absence of trypsin treatment but became sensitive to trypsin after 10 min of incubation (Fig. 2*C*). This indicated that removal of the outer membrane did not influence CRMP5 localization in the mitochondrial pellet, but it became sensitive to trypsin digestion. It should be noted that in isotonic buffer containing 0.07 M sucrose and 0.22 M mannitol CRMP5 was protected from trypsin proteolysis (Fig. 2*C*, *left panel*). These results argue in favor of CRMP5 localization on the inner mitochondrial membrane oriented toward the intermembrane space. To confirm the CRMP5 attachment to the membrane, sodium carbonate extraction, which allows the separation of the integral membrane proteins, was performed on the isolated mitochondria. Fig. 2*D* shows some CRMP5 protein in the supernatant containing peripheral proteins, whereas some CRMP5 was also in the insoluble protein fraction, *i.e.* attached to the inner mitochondrial membrane, as identified by the presence of a marker of the mitochondrial inner membrane, Tim23, in this fraction (Fig. 2*D*, *lower panel*). Together, these data suggest that

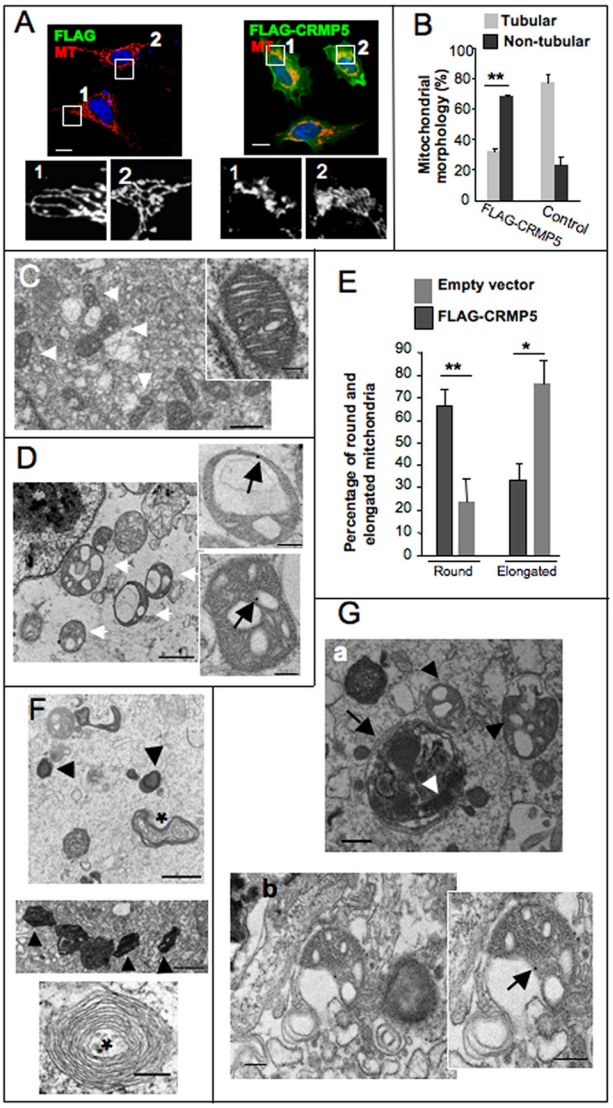

FIGURE 3. **CRMP5 modifies mitochondrial morphology.** *A*, SH-SY5Y cells with the particularity of having elongated mitochondria organized in a network are transfected with empty FLAG or FLAG-CRMP5 constructs. The cells are labeled with MT and anti-FLAG antibody and observed with fluorescence microscopy. The nucleus is *blue* with DAPI staining. Representative images of three independent experiments with similar results are shown. Mitochondrial morphology is scored as follows: tubular, long with higher interconnectivity; non-tubular, mainly small and round. *Left panels* show the control cells transfected with empty FLAG construct, and *right panels* show the CRMP5-transfected cells. High magnifications of *boxed areas 1* and *2* are shown in *white* in *bottom panels*. *Scale bars*, 20 μm. *B*, quantification of the number of non-tubular *versus* tubular mitochondria in cells. The number of mitochondria in each cell was individually counted using AxioVision Rel.4.8 software. Data are expressed as the percentage of tubular and non-tubular mitochondria in each cell ($n \geq 90$ cells per experiment). CRMP5-transfected cells present a higher percentage of non-tubular than tubular mitochondria (**, $p < 0.005$). Data are means ± S.E. *C–G*, CRMP5 overexpression induces the activation of the autophagic process. COS-7 cells were transfected with either FLAG or FLAG-CRMP5 vectors for 48 h, then fixed, and processed for electron microscopy as described under "Experimental Procedures." Representative images of at least four different experiments are shown. *C*, COS-7 cells transfected with the empty FLAG vector showing elongated mitochondria with typical ultrastructure (*white arrowheads*). *Scale bar*, 800 nm. The *right panel* shows high magnification of one mitochondrion. *Scale bar*, 200 nm. *D*, COS-7 cells transfected with FLAG-CRMP5 construct. The *white arrows* point to abnormal mitochondria that have lost their elongated morphology and appear more spherical. *Scale bar*, 800 nm. The *right two panels* show the magnification of one mitochondrion. *Black arrows* point to the immunogold particles, which label CRMP5 at the inner mitochondrial membrane. *Scale bar*, 200 nm. *E*, quantification of the number of round and elongated mitochondria in cells transfected with empty vector from *C* or FLAG-CRMP5 from *D*. The number of round and elongated mitochondria in each cell was individually counted. Data are expressed as the percentage of each type of mitochondria relative to the total number of mitochondria in CRMP5- ($n \geq 50$ cells in each experiment) *versus* FLAG-CRMP5-expressing cells ($n \geq 40$ cells in each experiment). The percentage of round mitochondria is higher in CRMP5- than in FLAG-CRMP5-transfected cells (**, $p < 0.005$). The percentage of elongated mitochondria is higher in FLAG-CRMP5- compared with CRMP5-expressing cells (*, $p < 0.01$). *F*, a mixture of numerous lysosomes (*black arrowheads*) and multilamellar bodies (*asterisks*) present in CRMP5-overexpressing cells (*upper panel*), indicating an increase in autophagic activity. *Scale bar*, 800 nm. The *middle panel* shows the presence of many lysosomes (9.26 ± 0.88/cell *versus* 4.18 ± 0.77/cell in empty vector-expressing cell; $n \geq 30$ cells in each experiment; $p < 0.005$). *Scale bar*, 800 nm. The *lower panel* shows a highly magnified lamellar body. *Scale bar*, 300 nm. *G*, in CRMP5-expressing cells, double membrane-limited structure in the autophage-lysosome pathway can be distinguished. *Upper panel a* shows double membrane-limited vacuole (*black arrow*) containing partly disintegrated mitochondria (*white arrowhead*). Note the presence of spherical mitochondria (*black arrowheads*). *Scale bar*, 500 nm. *Lower panel b* represents double membrane enveloping an intact mitochondrion, which may generate an autophagosome. The *black arrow* points to the immunogold particle labeling the CRMP5 at the mitochondrial membrane in high magnification of the image. *Scale bars*, 300 nm. *Error bars* represent S.E.

CRMP5 might interact strongly with the mitochondrial inner membrane and be directed toward the intermembrane space.

CRMP5 Affects Mitochondrial Morphology—The impact of CRMP5 on mitochondrial morphology was studied after transfection of SH-SY5Y neuroblastoma cells, which exhibit rather tubular and elongated mitochondria (34), with either FLAG or FLAG-CRMP5 vectors (Fig. 3*A*). In empty vector-transfected cells, the mitochondria appeared to be primarily tubular and organized in an interconnected network through the cell body (Fig. 3*A*, *left panels*). In contrast, the cells overexpressing FLAG-CRMP5 showed a clear change in their mitochondrial shape and distribution (Fig. 3*A*, *right panels*). First, mitochondria were mostly recruited in a perinuclear cluster. Second, the mitochondria appeared mainly small and round and lost their tubular shape. Quantification of the tubular *versus* non-tubular mitochondria showed that cells overexpressing CRMP5 protein have significantly fewer tubular (2.3-fold) than non-tubular mitochondria (Fig. 3*B*; **, $p < 0.005$), whereas the control cells exhibited a higher percentage of tubular than non-tubular mitochondria (78 *versus* 22%). Therefore, these data suggest that CRMP5 may be involved in the dynamics of mitochondrial morphology. To ascertain that the apparent fragmentation was not due to an artifact of overexpression, the CRMP5 expression was knocked down by siRNA (siCRMP5) in PC12 cells, which have the advantage of presenting a neuronal phenotype upon NGF stimulation. CRMP5 knockdown presenting an extent of about 60% depletion at the protein level triggered a more pronounced network of hyperfused tubular mitochondria compared with the control cells (data not shown).

To examine mitochondrial ultrastructure, we performed transmission electron microscopy in CRMP5-transfected COS-7 cells and observed different types of mitochondrial clusters. The empty vector-transfected cells presented typical mitochondrial morphology with rather elongated shape (Fig. 3*C*, *white arrowheads*). In contrast, in FLAG-CRMP5-transfected cells, mitochondria seemed to undergo major morphological changes, showing much less of a thin and tubular shape and appearing highly spherical. The cristae were intact, although the mitochondrial matrix was completely distorted (Fig. 3*D*,

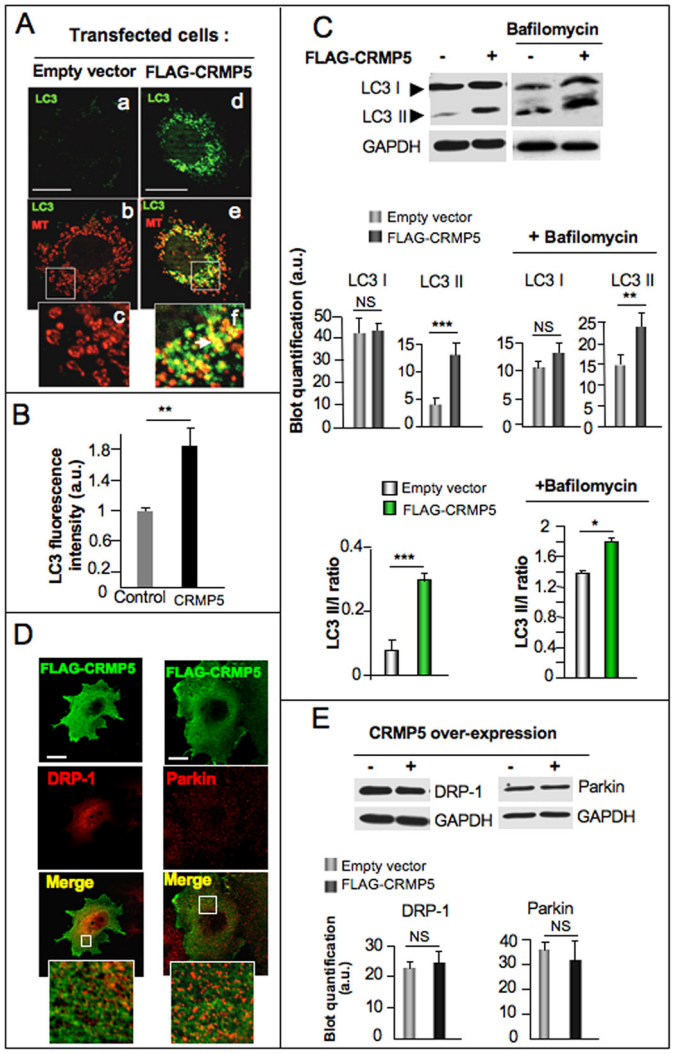

FIGURE 4. **CRMP5 overexpression causes an increase in LC3-II formation without any effect on DRP-1 and Parkin expression.** *A*, COS-7 cells transfected with FLAG (*panels a–c*) or FLAG-CRMP5 vectors (*panels d–f*) are labeled with MT (*red*) and anti-LC3 antibody (*green*) and observed by fluorescence microscopy. In CRMP5-transfected cells (*panel d*), clear LC3 labeling can be observed. *Insets* show high magnifications of the *boxed areas* in the merged images. The *yellow* puncta (*panel f*, *white arrow*) indicate the overlap between the LC3 and mitochondrial labeling. *Scale bars*, 20 μm. *B*, quantification of the fluorescence of LC3 protein. The *green* fluorescence intensity of each individual cell was obtained, using AxioVision Rel.4.8 software, from fluorescence microscopy images, and the mean fluorescence values of LC3-positive CRMP5-transfected cells are shown compared with the control empty vector-transfected cells for which the value was arbitrary set to 1.0. Data are means ± S.E. of three independent experiments ($n \geq 32$ cells in each experiment). **, $p < 0.005$. *C*, after transfection with either FLAG (−) or FLAG-CRMP5 (+) vectors for 48 h, COS-7 cells were incubated or not with 10 nM bafilomycin A1 for 2 h, and the total cell lysates were subjected to Western blot analysis using anti-LC3 antibody. GAPDH antibody is used as loading control. Note the increase in the expression of the LC3-II isoform upon CRMP5 overexpression at the protein level, whereas an identical amount of LC3-I can be observed in the presence or absence of CRMP5 overexpression (*upper left panels*). After bafilomycin A1 treatment, the overexpression of CRMP5 enhances the accumulation of LC3-II (*upper right panels*). The *middle panels* show quantitative densitometric analysis performed on LC3-I and LC3-II protein bands detected with anti-LC3 antibody. The band intensities at each condition were quantified to derive their relative intensity and normalized with GAPDH. Each result is representative of three separate experiments. Data, expressed in arbitrary units, are means ± S.E. The increase in LC3-II expression in CRMP5-transfected compared with empty vector-transfected cells can be observed in both the absence and presence of bafilomycin A1. ***, $p < 0.0001$; **, $p < 0.005$, respectively. *NS*, non-significant. *Bottom panels* show the LC3-II/LC3-I ratio derived from the mean values of the above densitometric analysis. This ratio is increased upon CRMP5 expression (***, $p < 0.0001$), and the increase is accentuated after bafilomycin A1 treatment (*, $p < 0.01$). *D*, COS-7 cells were transfected with FLAG-CRMP5 vector and double stained with both anti-FLAG (*green*) and anti-DRP-1 or anti-Parkin antibodies (*red*). *Insets* are high magnifications from the *boxed areas* in the merged images. The anti-FLAG antibody labeling does not overlap with anti-DRP-1 and anti-Parkin immunostaining. *Scale bars*, 20 μm. *E*, after transfection with either FLAG (−) or FLAG-CRMP5 (+) vectors, the total lysates of COS-7 cells were subjected to Western blot analysis using anti-DRP-1 or anti-Parkin antibodies as above (*upper panels*). The densitometric quantification of protein band intensities, normalized with GAPDH and expressed as arbitrary units, shows no significant changes in DRP-1 and Parkin expression when CRMP5 is overexpressed (*lower panels*). Each result is representative of three separate experiments. Data are means ± S.E. *NS*, non-significant. *Error bars* represent S.E.

white arrows). Note the specific gold particle labeling of CRMP5 at the mitochondrial membrane at high image magnifications (Fig. 3*D*, *black arrows*). Quantification of the tubular *versus* round mitochondria showed that cells overexpressing CRMP5 protein have a significantly higher percentage of round (2.7-fold) mitochondria than the empty vector-transfected control cells (Fig. 3*E*; **, $p < 0.005$), whereas the control cells presented a higher percentage of elongated mitochondria than the CRMP5-expressing cells (75 *versus* 24%). These observations suggest that CRMP5 may modify the mitochondrial network.

CRMP5 Expression Increases Autophagosome Expression—Transmission electron microscopy on CRMP5-transfected cells also revealed a significant increase (2.2-fold) in the number of lysosomes (Fig. 3*F*, *upper* and *middle panels*) and the appearance of numerous vesicles and lamellar bodies (Fig. 3*F*, *lower panel*) derived from autolysosomes after lysosomal degradation (35). Typical autophagic structures were observed in CRMP5-expressing cells (Fig. 3*G*). Double membrane-limited vacuoles containing disintegrated mitochondria were observed (Fig. 3*G*, *panel a*, *black arrow*). The *white arrowhead* points to the sequestered mitochondria. Other double membrane-limited structures could be identified. Inside those structures a mitochondrion seemed to be engulfed (Fig. 3*G*, *panel b*), indicative of a possible developing autophagosome. Gold particle labeling of CRMP5 at the mitochondrial membrane was highlighted in the high magnification of the image (Fig. 3*G*, *panel b*, *black arrow*). Together, these observations suggest a mitochondrial autophagic event. To confirm the induction of mitophagy by CRMP5, the first step was to check the localization of the most widely monitored autophagy-related protein, LC3, within the cell. Therefore, we performed double staining of the CRMP5-transfected cells with MT and the anti-LC3 antibody. In fact, LC3 can induce mitophagy only when translocated at the mitochondrial level (6). Distinct LC3 protein expression was observed in cells expressing CRMP5 (Fig. 4*A*, *panel d*) with a clear co-localization with MT (Fig. 4*A*, *panels e* and *f*, *white arrow*), whereas the control cells showed a weak LC3 expression (Fig. 4*A*, *panel a*). Quantification of LC3 fluorescence intensities showed a significant increase (1.8-fold) in LC3 staining in CRMP5-overexpressing cells compared with empty vector-transfected cells (Fig. 4*B*; **, $p < 0.005$), reflecting the increase in the number of autophagosomes localized at the mitochondrial level. In addition, Fig. 5*A* demonstrates that CRMP5 labeling co-localized with LC3 staining in CRMP5-expressing cells but not in the control FLAG-expressing cells. During autophagosome biogenesis, LC3 is covalently attached

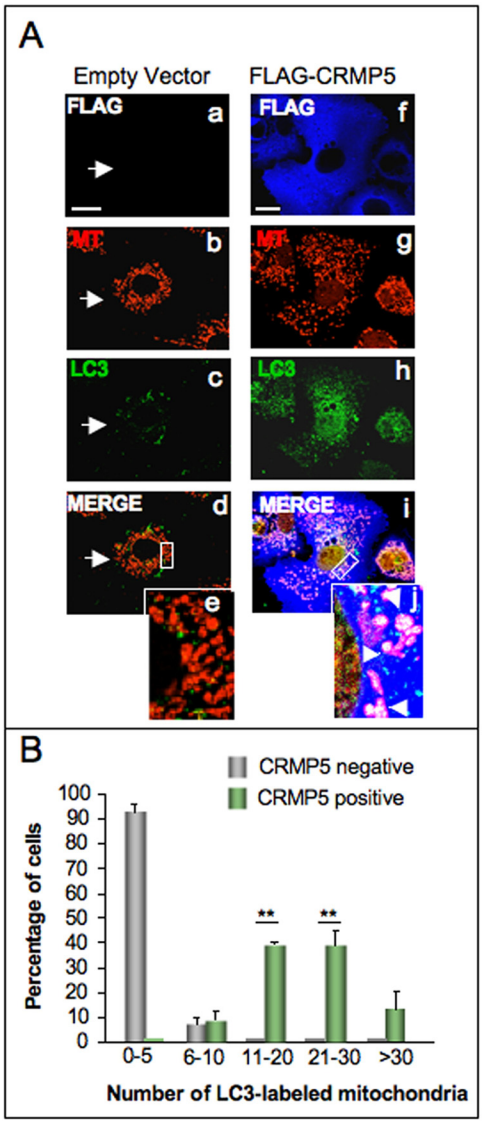

FIGURE 5. **CRMP5 induces LC3 translocation at the mitochondrial level.** *A*, COS-7 cells transfected with FLAG or FLAG-CRMP5 vectors were subjected to triple labeling with MT (*red*) and anti-FLAG (*blue*) and anti-LC3 (*green*) antibodies and observed by fluorescence microscopy. In the *left panels*, the control empty vector-transfected cells (*panels a–e*) show weak expression of LC3 protein. In cells overexpressing CRMP5 (*panels f–j*), LC3 and CRMP5 staining overlaps along mitochondria as *white* puncta (*panel j*; *white arrowheads* in the *inset*). *Scale bars*, 20 μm. *B*, the number of LC3 localized within mitochondria (dots/cell) was quantified in three independent experiments in CRMP5-positive cells (FLAG-CRMP5-transfected cells; $n \geq 30$ cells in each experiment) and -negative cells (empty vector-transfected cells; $n \geq 25$ cells in each experiment) and expressed as a percentage of cells exhibiting various numbers of mitochondria labeled with LC3. Data are means ± S.E. of three experiments. **, $p < 0.005$. *Error bars* represent S.E.

to phosphatidylethanolamine, giving rise to the membrane-bound LC3-II isoform (6); thus, the evaluation of changes in LC3-II isoform was essential. Western blot analysis of the cell extract showed a net increase in the expression of LC3-II in CRMP5-transfected cells compared with the control cells, although the level of LC3-I expression seemed not to change after CRMP5 expression (Fig. 4*C*, *upper left panel*). Quantitative analysis of the relative protein expression further confirmed that 1) the LC3-II expression was 3.5-fold higher in CRMP5-expressing cells than in control cells (Fig. 4*C*, *middle left panels*; ***, $p < 0.0001$) and 2) that the ratio of LC3-II/LC3-I was higher (3-fold) in CRMP5-expressing *versus* the control cells (Fig. 4*C*, *lower left panels*; ***, $p < 0.0001$). This increase in the conversion of LC3-I to the LC3-II isoform is a clear indicator of an increased number of autophagosomes. To strengthen that the increase of autophagosome number by CRMP5 is related to an enhancement of the autophagic flux, we evaluated LC3-II turnover by Western blot analysis in the presence and absence of bafilomycin A1, a potent and specific inhibitor of vacuolar H^+-ATPase, which blocks the fusion of autophagosomes with lysosomes, leading to autophagosome accumulation (36). Consequently, a higher ratio of LC3-II/LC3-I indicates the occurrence of the flux following bafilomycin A1 treatment. As expected, in bafilomycin-treated cells, the expression of LC3-II was higher in CRMP5-transfected cells than in control cells, although the basal level of LC3-II increased in control cells (Fig. 4*C*, *upper right panel*). Quantitative analysis of the protein expression showed that the accumulation of LC3-II in bafilomycin-treated CRMP5-transfected cells increased by1.6-fold compared with the control cells (Fig. 4*C*, *middle right panels*; **, $p < 0.005$), and the ratio of LC3-II/LC3-I reached 1.8 (1.2-fold higher than the control; *lower right panel*; *, $p < 0.01$). This increase in the conversion of LC3-I into the LC3-II isoform at the protein level after bafilomycin A1 treatment clearly strengthens an increase in autophagic flux upon CRMP5 expression.

The cellular distribution of CRMP5-overexpressing cells was also compared with that of other proteins known to be involved in mitochondrial dynamics and autophagy, such as Parkin whose mitochondrial translocation is known to be dependent on mitochondrial depolarization (2) and DRP-1, which promotes mitochondrial fission upon recruitment to the outer mitochondrial membrane (12). No CRMP5 overlap (stained *green*) with either DRP-1 or Parkin (stained *red*) could be observed upon FLAG-CRMP5 overexpression (stained *green*) as shown by distinct *green* and *red* staining under high magnification (Fig. 4*D*, *lower panels*). Moreover, Parkin labeling did not exhibit mitochondrial localization but remained uniformly distributed in the cytosol, whereas DRP-1 labeling occurred mostly at the perinuclear cluster. As expected, Western blot analysis showed that CRMP5 overexpression did not modify the level of expression of either DRP-1 or Parkin protein (Fig. 4*E*, *upper panels*). This is confirmed by quantitative analysis of protein expression (Fig. 4*E*, *lower panels*), suggesting that these two pathways are not involved in CRMP5-induced mitochondrial autophagy.

Next, we investigated whether the CRMP5 protein is located in mitochondria simultaneously with LC3 by triple labeling of cells using MT (stained *red*) and anti-FLAG (stained *blue*) and anti-LC3 (stained *green*) antibodies (Fig. 5*A*). CRMP5-transfected cells showed a large increase in LC3 expression (Fig. 5*A*, compare *panels c* and *h*) and its localization at the mitochondrial level (Fig. 5*A*, *panels g–j*) where it co-localized with CRMP5 as *white dots* observed at high magnification in the merged image (Fig. 5*A*, *panel j*, *white arrowheads*). When the number of LC3-labeled mitochondria was quantified and compared between empty vector- and CRMP5-transfected cells, unambiguously the total percentage of cells exhibiting high

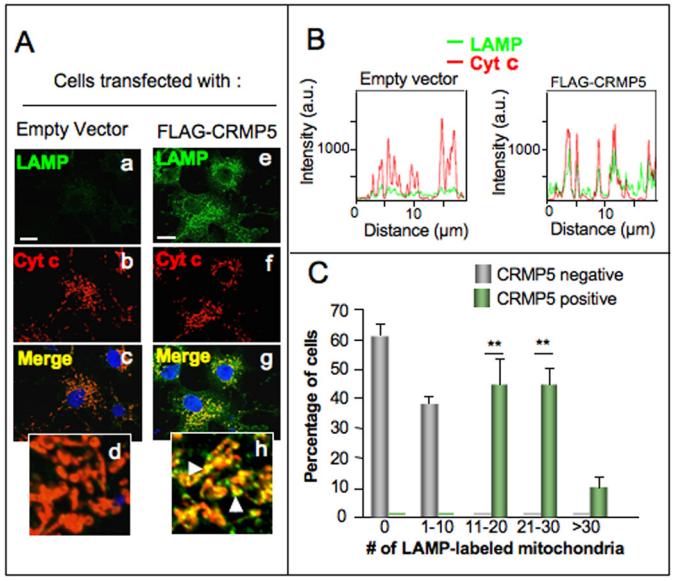

FIGURE 6. **CRMP5 induces and enhances mitophagy by recruiting lysosomes at the mitochondrial level.** *A*, COS 7 cells transfected with either FLAG or FLAG-CRMP5 vectors were double stained with anti-LAMP-2 (*green*) and anti-cytochrome *c* (*red*) antibodies and observed by fluorescence microscopy. The images are representative of three separate experiments with similar results. In the *left panels*, the control empty vector-transfected cells (*panels a–d*) show only cytochrome *c* labeling. In the *right panels*, the cells overexpressing CRMP5 (*panels e–h*) show clear overlapping of the LAMP-2 and cytochrome *c* staining along the mitochondria. *Scale bars*, 20 μm. *Insets* show high magnifications of the merged images. The nucleus is *blue* with DAPI staining. *Yellow* puncta (*white arrows*) indicate the co-localization of LAMP-2 and cytochrome *c* labeling, confirming that mitochondria are engaged in the mitophagy process. *B*, graphs showing the distribution of the *red* (cytochrome *c*) and *green* (LAMP-2) fluorescence intensities were obtained from *A* using AxioVision Rel.4.7.2.0 software. The superimposed *green* and *red* peaks indicate the co-localization of LAMP-2 and cytochrome *c* (*cyt c*) staining. *C*, quantification of the numbers of mitochondria (in three independent experiments) labeled with LAMP-2 antibody in CRMP5-positive ($n \geq 30$ cells in each experiment) and -negative ($n \geq 26$ cells in each experiment) cells. The number of LAMP-2-labeled mitochondria/cell is expressed as the percentage of cells showing various numbers of mitochondria labeled with the lysosomal marker. Data are means ± S.E. of three experiments. **, $p < 0.005$. *Error bars* represent S.E.

numbers of mitochondria labeled with LC3 (11–20, 21–30, or >30 labeled mitochondria/cell; Fig. 5*B*; **, $p < 0.005$) reached 86% in CRMP5-positive cells, whereas nearly 90% of CRMP5-negative cells had very low LC3 labeling within mitochondria (0–5 labeled mitochondria/cell; Fig. 5*B*). Collectively, these results clearly indicate that CRMP5, when recruited to mitochondria, leads to an increase in the number of autophagosomes, which are involved in mitophagy.

CRMP5 Expression Induces Lysosomal Translocation to the Mitochondrial Compartment and Enhances Mitophagy, Reducing the Mitochondrion Numbers—We then explored whether the increase in the number of autophagosome induced by CRMP5 overexpression was followed by their fusion with lysosomes to construct autolysosomes. Given that LAMP-2 is present both in lysosomes and autolysosomes, we performed double staining of CRMP5-transfected cells with anti-LAMP-2 and anti-cytochrome *c* antibodies to show the lysosomal docking at the mitochondrial level but not to other organelles. Empty vector-transfected COS-7 cells showed very faint anti-LAMP-2 staining (Fig. 6*A*, *panel a*). In contrast, CRMP5-expressing cells showed strong LAMP-2 labeling, which overlapped with cytochrome *c* immunostaining (Fig. 6*A*, *panels e–g*), indicating that the lysosomes were recruited at the mitochondrial level. The overlap is clearly identified by *yellow dots* in the high magnification of merged images (Fig. 6*A*, *panel h*, *white arrowheads*). The corresponding expression profiles were plotted based on the fluorescence intensities of LAMP-2 (stained *green*) and cytochrome *c* (stained *red*). This imaging analysis showed that in CRMP5-overexpressing cells, the majority of the *red* and *green* peaks were superimposed in the graph (Fig. 6*B*, *right panel*), indicating that lysosomes or autolysosomes are located at the mitochondrial level. In contrast, in control cells, analysis showed that LAMP-2 was poorly expressed (Fig. 6*B*, *left panel*). Quantification of LAMP-2-labeled mitochondria within each cell showed that in empty vector-transfected cells a small number of lysosomes overlapped with the mitochondrial labeling because nearly 60% of cells had no LAMP-2 labeling, and the remaining 40% showed only 1–10 LAMP-2-labeled mitochondria/cell (Fig. 6*C*, *gray bars*). However, all of the CRMP5-expressing cells showed a higher number of LAMP-2-labeled mitochondria because 36, 35, and 9% of cells exhibited 11–20, 21–30, and >30 LAMP-2-labeled mitochondria, respectively (Fig. 6*C*, *green bars*; **, $p < 0.005$). These results confirm that mitochondria are the target of numerous lysosomes; and thus, CRMP5 may be involved in the activation of mitophagy through its localization in mitochondria. To further elucidate the consequence of mitophagy induction by CRMP5, we studied the effect of CRMP5 expression on the extent of mitochondria over time. This experiment should confirm that the increased CRMP5-induced mitophagy is linked to a decreased proportion of mitochondria. CRMP5-expressing COS-7 cells showed elongated mitochondria 24 h post-transfection (Fig. 7*A*, *upper panels*), whereas at 48 h, fragmented mitochondria were observed (Fig. 7*A*, *middle panels*). At 72 h post-transfection, the mitochondria exhibited rather diffuse staining (Fig. 7*A*, *lower panels*). However, CRMP5 expression remained unchanged within 72 h as observed from the *green* fluorescence intensity in Fig. 7*A*, *upper*, *middle*, and *lower panels*. Quantification of *red* fluorescence intensity in CRMP5-expressing cells (Fig. 7*B*) showed a significant decrease (2.1-fold) in the mitochondrial fluorescence at 72 h of transfection compared with that at 24 h (**, $p < 0.005$), reflecting the decrease in the extent of mitochondria. These data collectively suggest that CRMP5 overexpression is linked with an increase of mitophagy, resulting in a reduction of mitochondrial content.

The Increase of Endogenous CRMP5 Expression in Hippocampal Neurons Negatively Affects the Mitochondrial Content in Dendrites—Because the removal of undamaged mitochondria can also occur during key developmental processes (6) and given that the endogenous CRMP5 exhibited a transient expression during the development of hippocampal neurons (27), we next investigated whether the change in endogenous CRMP5 expression could affect the mitochondrion numbers in neurons during development. Therefore, we studied the spatiotemporal distribution of mitochondria in dendrites and axon in cultured hippocampal neurons from E18 mouse embryos. The *in vitro* culture of hippocampal neurons could be considered as an excellent model to study the consequence of the fluctuation of CRMP5 expression in the physiological conditions. In such

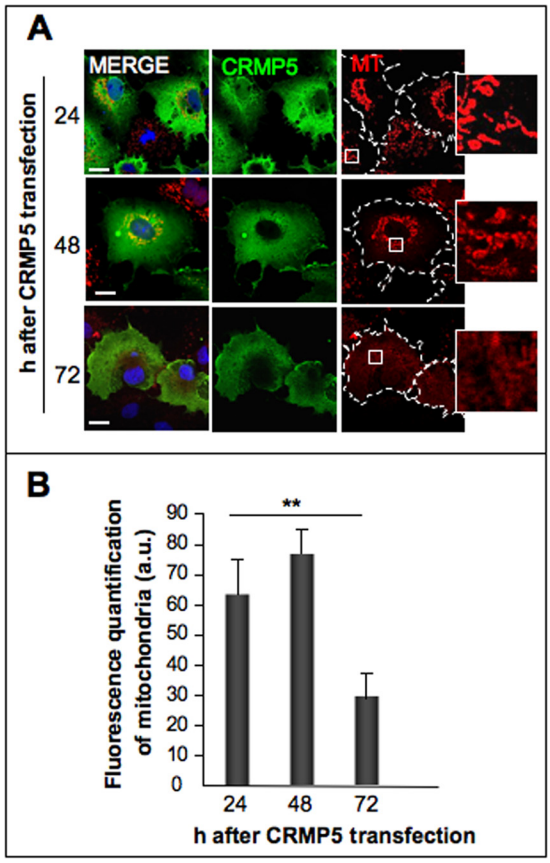

FIGURE 7. **CRMP5 expression reduces the extent of mitochondria over time.** *A*, COS-7 cells were transfected with FLAG-CRMP5 construct and maintained in culture for different lengths of time. The cells were labeled with MT (*red*) and anti-FLAG antibody (*green*) and observed by fluorescence microscopy. *Scale bars*, 20 μm. *Insets* show high magnifications of the MT images. At 48 h post-transfection, mitochondria are rather fragmented, whereas at 72 h post-transfection, mitochondria show very diffuse staining. *B*, quantification of the fluorescence intensity of MT labeling. The *error bars* indicate means ± S.E. in three separate experiments ($n \geq 10$ cells in each experiment). A clear decrease of fluorescence intensity can be observed after 72 h of transfection compared with 24–48 h, indicating an increase of mitophagy over time (**, $p < 0.005$). Data are expressed as a.u.

culture, Dotti *et al.* (37) have reported that a few days after axon began to grow remaining processes elongate and acquire the characteristic of dendrites. We previously have shown a transient expression of endogenous CRMP5 in hippocampal neurons; *i.e.* a high expression was observed in primary dendrites at DIV 3, maintaining the neurites in a quiescent state essential for axon elongation, whereas the poor CRMP5 expression on the following days suppressed the growth inhibition and allowed dendrite outgrowth (27). We compared the variation of endogenous expression of CRMP5 during neuritogenesis with that of mitochondrial content determined by MT labeling in dendrites and axon on DIV 2–5 (Fig. 8*A*). Fluorescence intensities indicative of CRMP5 expression and mitochondrial content were determined from defined regions on dendrites and axon using imaging software (ImageJ) and graphed as fluorescence values (Fig. 8*C*). First, a double staining of the neurons with anti-MAP2 (*cyan*) and anti-tau-1 (*green*) antibodies, specific markers of dendrites and axon, respectively, confirmed that the longest neurite was an axon and that the other neurites were dendrites (Fig. 8*B*). As expected, minor CRMP5 expression could only be detected in soma at DIV 2 (Fig. 8*A*, *panel a*), whereas at DIV 3, CRMP5 was strongly expressed in the soma and primary dendrites to maintain the dendrite inhibition during axonogenesis (Fig. 8*A*, *panel b*, and *C*; 13.4 ± 3.9 *versus* 1.21 ± 0.35 arbitrary units (a.u.) at DIV 2). During following stages corresponding to dendrite outgrowth, a decrease in CRMP5 expression was detected at DIV 4 followed by a very low expression level at DIV 5 (Fig. 8*A*, *panels c* and *d*, and *C*) consistent with our previous report (27). Strikingly, the mitochondrial content in the primary dendrites contrasted with CRMP5 expression because the *red* mitochondrial fluorescence was clearly detected in the soma and immature neurites at DIV 2 (Fig. 8*A*, *panel e*, and *C*), whereas mitochondrial labeling was clearly decreased at DIV 3 in the primary dendrites (Fig. 8*A*, *panel f*, and *C*; 3.7 ± 0.34 *versus* 8.1 ± 0.5 a.u. at DIV 2; ***, $p < 0.0001$). This suggested that high CRMP5 expression could be related to a reduction of mitochondrial numbers. At DIV 4, corresponding with a low CRMP5 expression, a 2.2-fold increase in mitochondrial staining was observed (Fig. 8*A*, *panel g*, and *B*; 8.1 ± 1.4 a.u.; **, $p < 0.005$) followed by a higher staining intensity at DIV 5 (Fig. 8*A*, *panel h*, and *B*; 14.3 ± 2.7 a.u.; **, $p < 0.005$). This indicated that high mitochondrial content could be correlated with a low CRMP5 expression. In contrast to dendrites, in the immature neurites, which began to elongate to become the future axon, the CRMP5 expression remained low and slightly decreased from DIV 3 to 5 in accordance with our previous study (27), but the mitochondrial labeling increased at DIV 4 and 5 as the axon elongated (Fig. 8*A*, *panels g* and *h*). Consistent with the data linking CRMP5 with mitophagy, these data inversely correlate the high expression of CRMP5 in primary dendrites with the extent of mitochondria.

Knockdown of CRMP5 Expression in Hippocampal Neurons Increases the Mitochondrion Numbers in Dendrites—To strengthen the above observation on the decrease of mitochondrial staining when CRMP5 is highly expressed, we knocked down CRMP5 expression in hippocampal neurons by siCRMP5 on day 1 after plating. Neurons were then examined 2 days after transfection at DIV 3 because a significant increase in CRMP5 expression was observed at this stage (see above). The immunostaining of endogenous CRMP5 in neurons treated with SC showed a clear *green* staining indicative of CRMP5 expression (Fig. 9*A*), whereas the absence of green staining in siCRMP5-treated cells revealed that CRMP5 expression was impaired (Fig. 9*B*). In SC-transfected cells, the mitochondria were restricted to the soma and axon because a low number of mitochondria were present at the dendritic level as observed in a high magnification image corresponding to MT staining (Fig. 9*A*). In contrast, the knockdown of CRMP5 in neurons drastically increased the MT staining in dendrites (Fig. 9*B*). The quantification of the number of mitochondria in dendrites indicated that the knockdown of CRMP5 induced a 1.8-fold increase in mitochondrial numbers at the dendritic level compared with the control SC-transfected neurons (Fig. 9*C*; *, $p < 0.01$). Similar results were obtained at the axon level (data not shown). These data indicate that in hippocampal neurons when the endogenous CRMP5 is highly expressed the mitochondrial numbers are unambiguously reduced, but the absence of

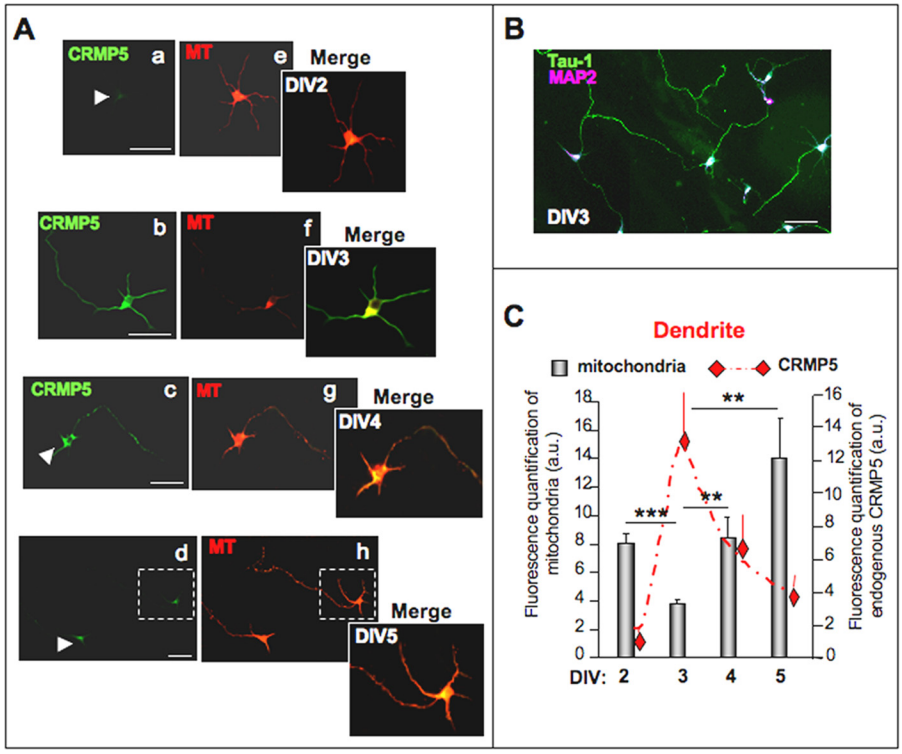

FIGURE 8. **Spatiotemporal expression of endogenous CRMP5 contrasted with the mitochondrion numbers in neurons.** Hippocampal neurons from E18 mouse were cultured from DIV 2 to 5. At each DIV, mitochondria were labeled with MT and then neurons were fixed and immunostained with anti-CRMP5 (*green*) to follow the distribution of endogenous CRMP5. Representative images of neurons from three different experiments are presented at each DIV. The *insets* highlight the magnification of the soma and dendrites in the merged image. *A*, at DIV 2, CRMP5 is restricted to the soma (*panel a*, *white arrowhead*), and the mitochondria are well detected in neurites (*panel e*), which are clearly stained *red* in the merge image. At DIV 3, CRMP5 expression is clearly detected in primary dendrites, axon, and soma (*panel b*) because a clear *green* staining can be observed in the merged image. The *red* staining of mitochondria unambiguously decreases at the dendritic level (*panel f*). *Scale bars*, 50 μm. From DIV 4–5, the CRMP5 expression decreases in dendrites (*panels c* and *d*, *white arrowheads*), whereas the MT staining of mitochondria strongly increases (*panels g* and *h*) as observed by the clear *red* staining in the merged image. Note that at these stages dendrites begin their growth. *Scale bars*, 50 μm. *B*, hippocampal neurons were stained with dendritic marker MAP2 (*cyan*) and axon marker tau-1 (*green*) antibodies to confirm that at DIV 3 the shorter neurites are dendrites and the longest neurite is an axon. *Scale bars*, 50 μm. *C*, quantification of CRMP5 and mitochondrial fluorescence in dendrites. The fluorescence intensity from *A* is determined after conversion of each fluorescent image into grayscale. Quantitative measurements are obtained by averaging the intensity of fluorescence within a box size of 40 $\times$ 40 pixels drawn on different regions of the dendrites ($n = 10$ measurement boxes within each neuron) using ImageJ software. Average fluorescence intensities obtained from these boxes in a number of neurons from three independent experiments are plotted in a.u. CRMP5 shows very low expression at DIV 2 ($n \geq 30$ neurons in each experiment), whereas MT fluorescence of mitochondria exhibits high intensity. A peak of CRMP5 expression at DIV 3 can be observed in accordance with previous results (27), whereas the MT fluorescence decreases compared with DIV 2 ($n \geq 24$ neurons; ***, $p < 0.0001$). MT staining increases at DIV 4 ($n \geq 25$ neurons; **, $p < 0.005$) and by 3.8-fold at DIV 5 compared with DIV 3 ($n \geq 20$ neurons; **, $p < 0.005$). This increase in mitochondrial staining is concomitant with a decrease of CRMP5 expression at DIV 4 and 5. All data shown are means $\pm$ S.E. *Error bars* represent S.E.

CRMP5 expression leads to higher mitochondrial numbers in dendrites.

DISCUSSION

Our results revealed two major findings concerning CRMP5, a cytosolic protein involved in brain development. First, we demonstrate the mitochondrial localization of CRMP5 in brain. Second, we provide evidence for a novel and unexpected role for this protein in the activation of mitophagy. Our results uncover a novel link between CRMP5 expression and reduction of mitochondrion numbers and further emphasize the importance of mitophagy process in controlling mitochondrion numbers during neuronal growth inhibition at the dendritic level.

Mitochondrial Translocation of CRMP5—In a screening for CRMP5-interacting protein, Takahashi *et al.* (38) identified a new septin, septin-4 (which they named M-septin), that shows mitochondrial localization. They suggested that CRMP5 could be translocated to mitochondria following septin overexpression. Here, we demonstrate that either endogenous or overexpressed CRMP5 protein can be directly localized within mitochondria. In addition, we show for the first time that, notwithstanding its cytosolic distribution, CRMP5 protein can be present *in vivo* in mitochondria isolated from mouse brain. Such mitochondrial localization for CRMP proteins has been reported previously only for CRMP2 and CRMP4 (39). An internal segment positioned in the N-terminal part of CRMP5 within residues 105–285 is responsible for its mitochondrial localization because CRMP5 ΔN285 and CRMP5 ΔN300 failed to localize to the mitochondrial compartment, whereas the full-length protein, CRMP5 ΔN104, and CRMP5 ΔC508 did. This is in perfect agreement with the presence of a buried segment located within β-strand 15 and α-helix 8 of the CRMP5 structure encompassing residues 239–260. The absence of a predicted mitochondrial targeting signal at the most N-terminal part of the protein is not unexpected because many proteins targeted to a mitochondrial subcompartment lack such sequence but instead have internal signals (40). The membrane insertion property of the protein was also confirmed in an *in*

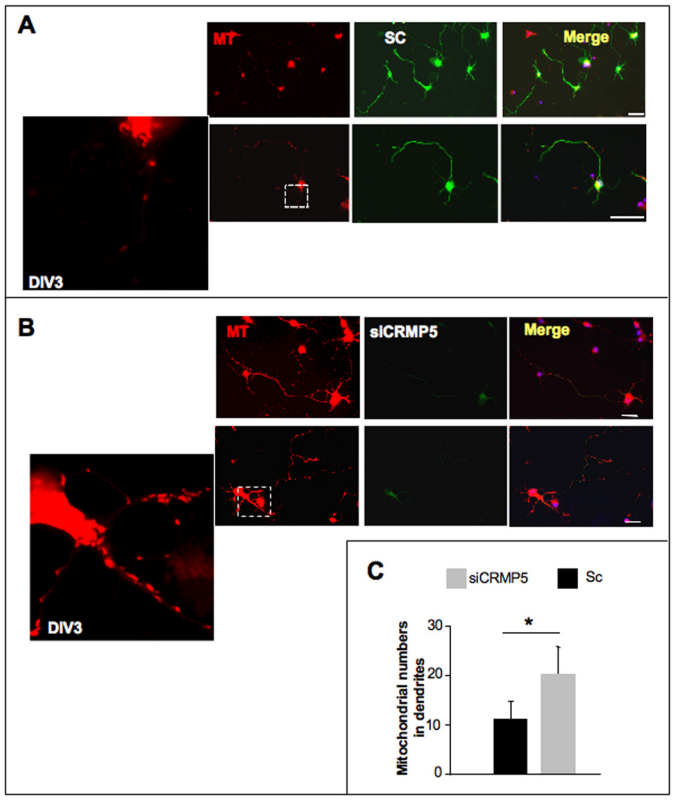

FIGURE 9. **CRMP5 depletion induces accumulation of mitochondria at dendritic level in cultured hippocampal neurons at DIV3.** *A* and *B*, mouse E18 hippocampal neurons were cultured for 1 day before transfection with either SC (*A*) or siCRMP5 (*B*). Two days later at DIV 3, mitochondria were labeled with 200 nM MT for 30 min, and then neurons were fixed and immunostained with anti-CRMP5 antibody (*green*). The nucleus is stained *blue* with DAPI in the merged images. Neurons were observed by fluorescence microscopy. Representative images from three independent experiments are presented, and the *insets* highlight the magnification of dendrites. *A*, endogenous CRMP5 expression is clearly detected in dendrites, axon, and the soma in SC-transfected control neurons at DIV 3 in *upper* and *lower panels* presenting different magnifications. The mitochondrial staining is restricted to the soma and axon. Very little MT staining is localized at the dendritic level as observed in the high magnifications of the *boxed area* in the *bottom panel*. *Scale bar*, 50 μm. *B*, the knockdown of CRMP5 by siCRMP5 induces a significant decrease of CRMP5 expression as evidenced by the faint *green* staining and results in increased mitochondrial staining. The *bottom panel* shows the magnification of the *boxed area*, highlighting increased MT staining in dendrites. *Scale bar*, 50 μm. *C*, the graph shows the quantification of the numbers of mitochondrion at the dendritic level in neurons. Neurons transfected with siCRMP5 ($n \geq 30$ neurons in each experiment) show an increase in the numbers of mitochondria present in dendrites compared with the control ($n \geq 40$ neurons in each experiment; *, $p < 0.01$). *Error bars* represent S.E.

vitro system by measuring the direct interaction of CRMP5 with a monomolecular film of DMPC. Interestingly, the maximal insertion pressure reaches 23 mN/m, a value not too different from the lateral pressure of 30 mN/m believed to correspond to the packing density of biological membranes (41).

Mitophagy Induction by CRMP5—Compelling evidence now suggests that the clearance of cell debris through autophagy is critical for human health. Indeed, autophagy is considered as an essential homeostatic process to clear misfolded or aggregated protein and to ensure organelle turnover (42). Dysfunctional autophagy has been implicated in a growing number of neurodegenerative diseases, including Parkinson disease, which shares the pathogenic pathways of mitochondrial abnormalities and misfolded protein damage (2, 43). Beyond quality control, mitophagy has also been shown to be involved in the removal of undamaged mitochondria during key developmental stages (6). Here, we provide evidence that under specific circumstances CRMP5 when highly expressed impairs mitochondrial morphology and dynamics and mobilizes the autophagy machinery. This is strengthened by the following observations. First, transmission electron microscopy clearly shows that CRMP5 overexpression generates a significant change in mitochondrial morphology with mitochondria appearing spherical rather than tubular. Second, CRMP5 expression enhances mitochondrial fragmentation, whereas CRMP5 depletion in cells exhibiting a neuronal phenotype prevents mitochondrial fragmentation, giving rise to elongated mitochondria. This mitochondrial fragmentation is consistent with mitophagy as several studies demonstrate that mitochondrial fission appears to be a prerequisite for mitophagy (1, 44, 45). Third, the overexpression of CRMP5 protein induces an increase in the expression of the LC3-II isoform, reflecting an increased number of autophagosomes, which is the hallmark of autophagy. Fourth, lysosomes are recruited at the mitochondrial level, causing their degradation over time. Increases in LC3-positive autophagosomes, measured in some studies by LC3 labeling, are often assessed by measuring the ratio of LC3-I over the membrane-bound LC3-II isoform using Western blot analysis (4, 45, 46). In our study, two complementary strategies based on immunofluorescence and Western blotting validate the CRMP5-induced increase in LC3 expression and clearly demonstrate an increase in the LC3-II/LC3-I ratio, supporting the formation of autophagosomes. This is strengthened by the fact that the inhibition of autophagic flux with bafilomycin A1 enhances the accumulation of LC3-II in CRMP5-expressing cells. Another argument, which strongly supports the assumption that the autophagic event occurs in the mitochondria, is the clear overlap of LC3 and CRMP5 at the mitochondrial level. Furthermore, following CRMP5 overexpression, lysosomal LAMP-2 overlaps with cytochrome *c*, demonstrating that lysosomes are recruited to the mitochondria to create autolysosomes formed by the fusion of autophagosomes and lysosomes, leading ultimately to the mitochondrial clearance. Because autophagy is a dynamic process that reflects both the formation of autophagosomes and their clearance subsequent to lysosomal fusion, the presence of numerous autophagosomes may reflect either an increase in formation or a decrease in their clearance. It is unlikely that CRMP5 overexpression leads to a decrease in autophagosome clearance because we demonstrate that mitochondrial content in these cells decreases over time, providing evidence that the lysosomal activity is enhanced. Altogether, our data clearly identify CRMP5 as a new actor in the complex processes of mitophagy.

A number of factors have been found to affect mitochondrial clearance during developmental or pathological process. Among them, PINK1, which is involved in mitochondrial fission, has been reported to modulate mitochondrial dynamics and to promote autophagy (44, 45). PINK1 and Nix contribute to mitochondrial priming by controlling the mitochondrial translocation of Parkin (15, 16, 44, 45). The molecular mechanisms regulating mitochondrial Parkin translocation have been reported to be dependent on loss of $\Delta\Psi_m$ (2). However, we

show that CRMP5 expression does not induce Parkin translocation in mitochondria and has no effect on Parkin expression. These observations were strengthened by the fact that, whereas Parkin translocation occurs in depolarized mitochondria, CRMP5 labels the $\Delta\Psi_m$ intact mitochondria because CRMP5 staining overlaps with MT, a dye able to stain specifically the polarized mitochondria. In the same way, CRMP5 expression has no effect on fission GTPase DRP-1 expression and localization. DRP-1 promotes mitochondrial fission upon recruitment to the outer mitochondrial membrane by the protein Fis (12). Therefore, CRMP5 may act in mitophagy by a new pathway different from the PINK1/Parkin- or DRP-1-directed pathways. In addition, the fact that all the above factors act at the level of the outer mitochondrial membrane, whereas detailed analyses of the submitochondrial location of CRMP5 in brain cortex show its attachment to the inner mitochondrial membrane, argues in favor of a different mechanism of action.

Recent findings have shown that during starvation mitochondrially derived membranes are used to supply membranes for autophagosome formation, and this has uncovered a mechanism involving the outer mitochondrial membrane without autophagic activation (47). Taking into account 1) its localization on the inner membrane and 2) that CRMP5 expression recruits lysosomes to the mitochondria leading *in fine* to autophagic degradation, it is unlikely that CRMP5 is involved in transferring mitochondrial lipids to autophagosomal membranes. Nonetheless, the possibility that, following a yet unknown stimulus, CRMP5 may induce some reorganization of the lipid in the inner membrane, thereby initiating the autophagic process, cannot be completely ruled out. This assumption is in accordance with our observation showing that, besides lipid monolayer penetration, CRMP5 was able to reorganize the condensed domains of phospholipids in the lipid layer.[3]

Physiological Significance of CRMP5-induced Mitophagy—CRMP5 was recently shown to inhibit dendritic growth at the early stages of neuronal development and to regulate neuronal polarity by maintaining the dendrites in a quiescent stage during axon outgrowth. Dendritic growth is regulated by the transient expression of endogenous CRMP5 and is inhibited by an increase of CRMP5 expression at the dendritic level (27). Here, we confirm that CRMP5 tightly controls this process by a parallel pathway implying mitophagy. In hippocampal neurons in culture, a correlation exists between high CRMP5 expression and the decrease of mitochondrial content in dendrites at stage 3 when dendrite outgrowth is inhibited. Moreover, the knockdown of CRMP5 at this stage induces an enhancement of the mitochondrion numbers. Subsequently, the absence of CRMP5 expression at stage 4 of neuronal development, corresponding to dendrite outgrowth (37), clearly coincides with a multiplication of mitochondrion numbers, suggesting that, in physiological conditions, the expression of CRMP5 and the subsequent mitophagy may play a role in the adjustment of the mitochondrion numbers in dendrites. These findings are consistent with previous studies on the removal of undamaged mitochondria during key developmental stages (6) and showing that mitophagy is involved in steady-state turnover of mitochondria (48). Taking into consideration that (i) CRMP5 plays a role in the inhibition of dendrite growth, counteracting the function of CRMP2; (ii) this inhibition is mediated by the tubulin binding property of CRMP5, which inhibited its polymerization; and (iii) the function of this inhibitory effect is to maintain neurites in a quiescent state at early stages of development (27), one can argue that in physiological conditions the strong expression of CRMP5 may have a relevant role in controlling and adjusting the mitochondrial number by promoting mitophagy and thereby can contribute to prevent tubulin polymerization by restraining energy formation. Thus, the induction of the mitophagy process in neurons during development may be an additional pathway for CRMP5 to reinforce its inhibition of dendritic growth, a very important step leading to the establishment of neuronal polarity and axonogenesis. Supporting our data, very recent studies on mitochondrial content in dendrites have also shown that sufficient dendritic mitochondrial content is required for proper dendritic morphological characteristics (49), acute decreases in dendritic mitochondria rapidly lead to synapse and spine loss (50), and chronic genetic stress leading to mitochondrial degradation via mitophagy can elicit dendrite shortening (51). In conclusion, CRMP5 presents a novel class of molecules involved in the control of steady-state mitochondrial number that are required to meet metabolic demand during specialized development stages. Further studies are needed to shed light on the molecular mechanisms that govern this new CRMP5 function and the signal that triggers the CRMP5-induced mitophagy.

Acknowledgments—We thank Dr. Olivier Pascual for critical reading of the manuscript. We are also thankful to Dr. Valérie Perrot for kindly providing us with different types of HA-tagged CRMP5 expression vectors.

[3] S. Menigoz, A. Girard-Egrot, and M. Moradi-Améli, unpublished observations.

REFERENCES

1. Twig, G., Elorza, A., Molina, A. J., Mohamed, H., Wikstrom, J. D., Walzer, G., Stiles, L., Haigh, S. E., Katz, S., Las, G., Alroy, J., Wu, M., Py, B. F., Yuan, J., Deeney, J. T., Corkey, B. E., and Shirihai, O. S. (2008) Fission and selective fusion govern mitochondrial segregation and elimination by autophagy. *EMBO J.* **27,** 433–446
2. Narendra, D., Tanaka, A., Suen, D. F., and Youle, R. J. (2008) Parkin is recruited selectively to impaired mitochondria and promotes their autophagy. *J. Cell Biol.* **183,** 795–803
3. Burbulla, L. F., Krebiehl, G., and Krüger, R. (2010) Balance is the challenge—the impact of mitochondrial dynamics in Parkinson's disease. *Eur. J. Clin. Invest.* **40,** 1048–1060
4. Rodríguez-Hernández, A., Cordero, M. D., Salviati, L., Artuch, R., Pineda, M., Briones, P., Gómez Izquierdo, L., Cotán, D., Navas, P., and Sánchez-Alcázar, J. A. (2009) Coenzyme Q deficiency triggers mitochondria degradation by mitophagy. *Autophagy* **5,** 19–32
5. Kanki, T., and Klionsky, D. J. (2010) The molecular mechanism of mitochondria autophagy in yeast. *Mol. Microbiol.* **75,** 795–800
6. Youle, R. J., and Narendra, D. P. (2011) Mechanism of mitophagy. *Nat. Rev. Mol. Cell Biol.* **12,** 9–14
7. Kabeya, Y., Mizushima, N., Ueno, T., Yamamoto, A., Kirisako, T., Noda, T., Kominami, E., Ohsumi, Y., and Yoshimori, T. (2000) LC3, a mammalian homologue of yeast Apg8p, is localized in autophagosome membranes after processing. *EMBO J.* **19,** 5720–5728
8. Tanida, I., Ueno, T., and Kominami, E. (2004) Human light chain

3/MAP1LC3B is cleaved at its carboxyl-terminal Met^{121} to expose Gly^{120} for lipidation and targeting to autophagosomal membranes. *J. Biol. Chem.* **279,** 47704–47710
9. Kroemer, G., and Levine, B. (2008) Autophagic cell death: the story of a misnomer. *Nat. Rev. Mol. Cell Biol.* **9,** 1004–1010
10. Liu, X., Feng, L., Yan, M., Xu, K., Yu, Y., and Zheng, X. (2010) Changes in mitochondrial dynamics during amyloid β-induced PC12 cell apoptosis. *Mol. Cell. Biochem.* **344,** 277–284
11. Cho, D. H., Nakamura, T., and Lipton, S. A. (2010) Mitochondrial dynamics in cell death and neurodegeneration. *Cell. Mol. Life Sci.* **67,** 3435–3447
12. Young, K. W., Piñon, L. G., Bampton, E. T., and Nicotera, P. (2010) Different pathways lead to mitochondrial fragmentation during apoptotic and excitotoxic cell death in primary neurons. *J. Biochem. Mol. Toxicol.* **24,** 335–341
13. Dawson, T. M., and Dawson, V. L. (2010) The role of parkin in familial and sporadic Parkinson's disease. *Mov. Disord.* **25,** S32–39
14. Tanaka, A. (2010) Parkin-mediated selective mitochondrial autophagy, mitophagy: Parkin purges damaged organelles from the vital mitochondrial network. *FEBS Lett.* **584,** 1386–1392
15. Geisler, S., Holmström, K. M., Skujat, D., Fiesel, F. C., Rothfuss, O. C., Kahle, P. J., and Springer, W. (2010) PINK1/Parkin-mediated mitophagy is dependent on VDAC1 and p62/SQSTM1. *Nat. Cell Biol.* **12,** 119–131
16. Ding, W. X., Ni, H. M., Li, M., Liao, Y., Chen, X., Stolz, D. B., Dorn G. W., 2nd, Yin, X. M. (2010) Nix is critical to two distinct phases of mitophagy, reactive oxygen species-mediated autophagy induction and Parkin-ubiquitin-p62-mediated mitochondrial priming. *J. Biol. Chem.* **285,** 27879–27890
17. Wang, L. H., and Strittmatter, S. M. (1997) Brain CRMP forms heterotetramers similar to liver dihydropyrimidinase. *J. Neurochem.* **69,** 2261–2269
18. Inatome, R., Tsujimura, T., Hitomi, T., Mitsui, N., Hermann, P., Kuroda, S., Yamamura, H., and Yanagi, S. (2000) Identification of CRAM, a novel unc-33 gene family protein that associates with CRMP3 and protein-tyrosine kinase(s) in the developing rat brain. *J. Biol. Chem.* **275,** 27291–27302
19. Goshima, Y., Nakamura, F., Strittmatter, P., and Strittmatter, S. M. (1995) Collapsin-induced growth cone collapse mediated by an intracellular protein related to UNC-33. *Nature* **376,** 509–514
20. Fukata, Y., Itoh, T. J., Kimura, T., Ménager, C., Nishimura, T., Shiromizu, T., Watanabe, H., Inagaki, N., Iwamatsu, A., Hotani, H., and Kaibuchi, K. (2002) CRMP-2 binds to tubulin heterodimers to promote microtubule assembly. *Nat. Cell Biol.* **4,** 583–591
21. Kimura, T., Watanabe, H., Iwamatsu, A., and Kaibuchi, K. (2005) Tubulin and CRMP-2 complex is transported via Kinesin-1. *J. Neurochem.* **93,** 1371–1382
22. Arimura, N., Kimura, T., Nakamuta, S., Taya, S., Funahashi, Y., Hattori, A., Shimada, A., Ménager, C., Kawabata, S., Fujii, K., Iwamatsu, A., Segal, R. A., Fukuda, M., and Kaibuchi, K. (2009) Anterograde transport of TrkB in axons is mediated by direct interaction with Slp1 and Rab27. *Dev. Cell* **16,** 675–686
23. Veyrac, A., Reibel, S., Sacquet, J., Mutin, M., Camdessanche, J. P., Kolattukudy, P., Honnorat, J., and Jourdan, F. (2011) CRMP5 regulates generation and survival of newborn neurons in olfactory and hippocampal neurogenic areas of the adult mouse brain. *PLoS One* **6,** e23721
24. Ricard, D., Rogemond, V., Charrier, E., Aguera, M., Bagnard, D., Belin, M. F., Thomasset, N., and Honnorat, J. (2001) Isolation and expression pattern of human Unc-33-like phosphoprotein 6/collapsin response mediator protein 5 (Ulip6/CRMP5): coexistence with Ulip2/CRMP2 in Sema3a-sensitive oligodendrocytes. *J. Neurosci.* **21,** 7203–7214
25. Hotta, A., Inatome, R., Yuasa-Kawada, J., Qin, Q., Yamamura, H., and Yanagi, S. (2005) Critical role of collapsin response mediator protein-associated molecule CRAM for filopodia and growth cone development in neurons. *Mol. Biol. Cell* **16,** 32–39
26. Yamashita, N., Mosinger, B., Roy, A., Miyazaki, M., Ugajin K., Nakamura F., Sasaki, Y., Yamaguchi, K., Kolattukudy, P., and Goshima, Y. (2011) CRMP5 (collapsin response mediator protein 5) regulates dendritic development and synaptic plasticity in the cerebellar Purkinje cells. *J. Neurosci.* **31,** 1773–1779
27. Brot, S., Rogemond, V., Perrot, V., Chounlamountri, N., Auger, C., Honnorat, J., and Moradi-Améli, M. (2010) CRMP5 interacts with tubulin to inhibit neurite outgrowth, thereby modulating the function of CRMP2. *J. Neurosci.* **30,** 10639–10654
28. Ponnusamy, R., and Lohkamp, B. (2013) Insights into the oligomerization of CRMPs: crystal structure of human collapsing response mediator protein 5. *J. Neurochem.* **125,** 855–868
29. Honnorat, J., Cartalat-Carel, S., Ricard, D., Camdessanche, J. P., Carpentier, A. F., Rogemond, V., Chapuis, F., Aguera, M., Decullier, E., Duchemin, A. M., Graus, F., and Antoine J. C. (2009) Onco-neural antibodies and tumor type determine survival and neurological symptoms in paraneoplastic neurological syndromes with Hu or CV2/CRMP5 antibodies. *J. Neurol. Neurosurg. Psychiatry* **80,** 412–416
30. Rogemond, V., Auger, C., Giraudon, P., Becchi, M., Auvergnon, N., Belin, M. F., Honnorat, J., and Moradi-Améli, M. (2008) Processing and nuclear localization of CRMP2 during brain development induce neurite outgrowth inhibition. *J. Biol. Chem.* **283,** 14751–14761
31. Guillemin, Y., Lopez, J., Gimenez, D., Fuertes, G., Valero, J. G., Blum, L., Gonzalo, P., Salgado, J., Girard-Egrot, A., and Aouacheria, A. (2010) Fragments from pro- and antiapoptotic BCL-2 proteins have distinct membrane behavior reflecting their functional divergence. *PLoS One* **5,** e9066
32. Daum, G. (1985) Lipids of mitochondria. *Biochim. Biophys. Acta* **822,** 1–42
33. Maggio, B. (1994) the surface behavior of glyco-sphingolopids in biomembranes: a new frontier of molecular ecology. *Prog. Biophys. Mol. Biol.* **62,** 55–117
34. Lutz, A. K., Exner, N., Fett, M. E., Schlehe, J. S., Kloos, K., Lämmermann, K., Brunner, B., Kurz-Drexler, A., Vogel, F., Reichert, A. S., Bouman, L., Vogt-Weisenhorn, D., Wurst, W., Tatzelt, J., Haass, C., and Winklhofer, K. F. (2009) Loss of parkin or PINK 1 function increases Drp1-dependent mitochondrial fragmentation. *J. Biol. Chem.* **284,** 22938–22951
35. Lajoie, P., Guay, G., Dennis, J. W., and Nabi, I. R. (2005) The lipid composition of autophagic vacuoles regulates expression of multilamellar bodies. *J. Cell Sci.* **118,** 1991–2003
36. Yamamoto, A., Tagawa, Y., Yoshimori, T., Moriyama, Y., Masaki, R., and Tashiro, Y. (1998) Bafilomycin A1 prevents maturation of autophagic vacuoles by inhibiting fusion between autophagosomes and lysosomes in rat hepatoma cell line, H-4-II-E cells. *Cell Struct. Funct.* **23,** 33–42
37. Dotti, C. G., Sullivan, C. A., and Banker, G. A. (1988) Establishment of polarity by hippocampal neurons in culture. *J. Neurosci.* **8,** 1454–1468
38. Takahashi, S., Inatome, R., Yamamura, H., and Yanagi, S. (2003) Isolation and expression of a novel mitochondrial septin that interacts with CRMP/CRAM in the developing neurons. *Genes Cells* **8,** 81–93
39. Rembutsu, M., Soutar, M. P., Van Aalten, L., Gourlay, R., Hastie, C. J., McLauchlan, H., Morrice, N. A., Cole, A. R., and Sutherland, C. (2008) Novel procedure to investigate the effect of phosphorylation on protein complex formation *in vitro* and in cells. *Biochemistry* **47,** 2153–2161
40. Neupert, W., and Herrmann, J. M. (2007) Translocation of proteins into mitochondria. *Annu. Rev. Biochem.* **76,** 723–749
41. Marsh, D. (1996) Lateral pressure in membranes. *Biochim. Biophys. Acta* **1286,** 183–223
42. Mizushima, N., Yamamoto, A., Matsui, M., Yoshimori, T., and Ohsumi, Y. (2004) *In vivo* analysis of autophagy in response to nutrient starvation using transgenic mice expressing a fluorescent autophagosome marker. *Mol. Biol. Cell* **15,** 1101–1111
43. Komatsu, M., Ueno, T., Waguri, S., Uchiyama, Y., Kominami, E., and Tanaka, K. (2007) Constitutive autophagy: vital role in clearance of unfavourable proteins in neurons. *Cell Death Differ.* **14,** 887–894
44. Yang, Y., Ouyang, Y., Yang, L., Beal, M. F., McQuibban, A., Vogel, H., and Lu, B. (2008) Pink1 regulates mitochondrial dynamics through interaction with the fission/fusion machinery. *Proc. Natl. Acad. Sci. U.S.A.* **105,** 7070–7075
45. Michiorri, S., Gelmetti, V., Giarda, E., Lombardi, F., Romano, F., Marongiu, R., Nerini-Molteni, S., Sale, P., Vago, R., Arena, G., Torosantucci, L., Cassina, L., Russo, M. A., Dallapiccola, B., Valente, E. M., and Casari, G. (2010) The Parkinson-associated protein PINK1 interacts with Beclin 1 and promotes autophagy. *Cell Death Differ.* **17,** 962–974
46. Kim, J., Huang, W. P., and Klionsky, D. J. (2001) Membrane recruitment of

Aut7p in the autophagy and cytoplasm to vacuole targeting pathways requires Aut1p, Aut2p, and the autophagy conjugation complex. *J. Cell Biol.* **152,** 51–64
47. Hailey, D. W., Rambold, A. S., Satpute-Krishnan, P., Mitra, K., Sougrat, R., Kim, P. K., and Lippincott-Schwartz, J. (2010) Mitochondria supply membrane for autophagosome biogenesis during starvation. *Cell* **141,** 656–667
48. Tal, R., Winter, G., Ecker, N., Klionsky, D. J., and Abeliovich, H. (2007) Aup1p a yeast mitochondrial protein phosphatase homolog, is required for efficient stationary phase mitophagy and cell survival. *J. Biol. Chem.* **282,** 5617–5624
49. Mattson, M. P., Gleichmann, M., and Cheng, A. (2008) Mitochondria in neuroplasticity and neurological disorders. *Neuron* **60,** 748–766
50. Li, Z., Okamoto, K., Hayashi, Y., and Sheng, M. (2004) The importance of dendritic mitochondria in the morphogenesis and plasticity of spines and synapses. *Cell* **119,** 873–887
51. Cherra, S. J., 3rd, Steer, E., Gusdon, A. M., Kiselyov, K., and Chu, C. T. (2013) Mutant *LRRK2* elicits calcium imbalance and depletion of dendritic mitochondria in neurons. *Am. J. Pathol.* **182,** 474–484